

COMPUTATION OF \wp -FUNCTIONS ON PLANE ALGEBRAIC CURVES

J BERNATSKA

ABSTRACT. Numerical tools for computation of \wp -functions, also known as Kleinian, or multiply periodic, are proposed. In this connection, computation of periods of the both first and second kinds is reconsidered. An analytical approach to constructing Riemann surfaces of plane algebraic curves of low gonality is used. The approach is based on explicit radical solutions to quadratic, cubic, and quartic equations, which serve for hyperelliptic, trigonal, and tetragonal curves, respectively. The proposed analytical models of Riemann surfaces give full control over computation of the Abel image of any point or divisor. Therefore, computation of \wp -functions at Abel images of given divisors can be done directly. An alternative computation with the help of the Jacobi inversion problem is used for verification. Hyperelliptic and trigonal curves are considered in detail, and illustrated by examples. A method of finding the unique characteristic corresponding to the vector of Riemann constants is suggested for non-hyperelliptic and hyperelliptic curves.

Keywords: uniformization, sigma function, multiply periodic functions, Riemann surface model, vector of Riemann constants

MSC: 32Q30, 30F10, 33F05, 65D20

1. INTRODUCTION

The interest to computing \wp -functions, also known as Kleinian after [10], or multiply periodic after [3], arises from the realm of completely integrable systems, e.g. the hierarchies of the Korteweg—de Vries equation (KdV), the sine-Gordon equation (SG), the non-linear Schrödinger equation (NLS), etc., since finite-gap solutions can be expressed in terms of these functions, see [10, 6]. Such a representation of solutions is rarely used, and convenient tools for computation are not developed.

Direct computation of $\wp_{1,1}$ -function as a solution of the KdV equation is applied in [6]. Since solutions are required to be real-valued, $\wp_{1,1}$ -function is computed along a particular path in the Jacobian variety of a spectral curve.

An alternative way of computing solutions of the mKdV, and KdV equations can be found in [20, 21]. Though a solution in terms of $\wp_{1,1}$ -function is used, it is expressed in terms of a divisor on a hyperelliptic curve which solves the Jacobi inversion problem. Thus, the required solution is obtained from computation of the inverse of the Abel map by means of Euler's numerical quadrature. Computation of periods on a curve is avoided, as well as direct computation of $\wp_{1,1}$ -function.

On the other hand, solutions of completely integrable equations in term of theta functions, see for example [4], are widely used. And numerical tools for computation of the Riemann period matrix and the theta function are well developed.

Date: January 7, 2025.

A powerful method of computing first kind period matrices (normalized and not normalized) associated with a given plane curve was presented in [12], and implemented in the Maple package `algcurves`, see a detailed description in [13]. Also other packages for computing first kind period matrices, the Abel map, and the theta function and its derivatives are created in Sage, Matlab, Julia, see [1] for a brief review.

Computation with the help of spectral approximation is suggested in [17]. Linear combinations of Chebyshev polynomials are used in approximation of integrands of first and third kind integrals between branch points, and integration is performed with the help of the orthogonality relation on the polynomials. Numerical simulation is performed in Matlab. With Riemann period matrices computed by means of this technique, solutions of the KdV and KP equations on hyperelliptic curves of genera 2, 4, 6 are computed and illustrated in [18]. Solutions of the NLS equation and the Davey–Stewartson equation on hyperelliptic curves of genera 2 and 4 are presented in [19]. The spectral approximation technique allows to increase accuracy in almost solitonic cases, when pairs of branch points collide.

The known numerical tools are designed for studying theta-functional solutions. On the contrary, computation of \wp -functions is lacking for appropriate numerical tools. First of all, periods of the both first and second kinds, subject to the Legendre relation, are required. These periods are obtained from first and second kind differentials which form an associated¹ system. Second kind periods are not covered by the known packages. Therefore, particular attention will be paid to computation of first and second kind periods on algebraic curves in question.

The problem of verifying results of computation gave rise to developing analytical models of Riemann surfaces of plane algebraic curves of low gonality. Such a model is constructed from explicit solutions obtained as radical expressions for roots of a quadratic, cubic, or quartic equation, which serves for a hyperelliptic, trigonal, or tetragonal curve, respectively. Continuous connection between these solutions is described analytically in whole. The obtained analytical model of a Riemann surface gives a full understanding how to compute the Abel image of any point of the corresponding curve. So, an effective analytical method of direct computation on plane algebraic curves of low gonality is proposed.

This analytical approach was initiated by V. Enolsky, and the hyperelliptic case with real branch points was developed by him. First and second kind periods obtained by this method served for verification of relations on theta functions, and \wp -functions. However, the method had never been published before. In the present paper the method is extended to hyperelliptic curves with arbitrary complex branch points, and to trigonal curves. These two types of plane algebraic curves are the most demanded. In fact, only integrable systems with hyperelliptic spectral curves have been considered in the literature as a matter of computation.

In addition to direct computation of \wp -functions, computation based on the Jacobi inversion problem is also presented. The latter is used for verification that obtained values of \wp -functions are correct, and periods used for computing \wp -functions accommodate the curve in question. In the hyperelliptic case, generalizations of the Bolza formulas, which give expressions for branch points in terms of theta functions with characteristics, are used for verification of computed periods.

¹Fundamental integrals of the second kind associated with the standard not normalized first kind integrals were introduced in [2, § 138].

The paper is organized as follows. In Preliminaries the notion of Sato weight, the definitions of σ -function and \wp -functions are given, and also the Bolza formulas, and solutions of the Jacobi inversion problem on hyperelliptic and trigonal curves. In section 3 an analytical model of the Riemann surface of a hyperelliptic curve, and computation of periods are explained in detail. Section 4 shows computation of the Abel images of arbitrary points of a hyperelliptic curve, and \wp -functions on non-special divisors. In section 5 an analytical model of the Riemann surface of a trigonal curve and computation of periods are presented. Section 6 illustrates the trigonal case with computations of the Abel images of arbitrary points, and \wp -functions.

The proposed method is illustrated by examples: hyperelliptic curves of genus 4 with (1) complex branch points, and (2) all real branch points, and a trigonal curve of genus 3. Computations are made in Wolfram Mathematica 12. The full code is posted in the Wolfram Community portal, see

<https://community.wolfram.com/groups/-/m/t/3243472>

<https://community.wolfram.com/groups/-/m/t/3252458>

2. PRELIMINARIES

2.1. Sato weight. The notion of *Sato weight* plays an important role in the theory of (n, s) -curves. Such a curve arises as a universal unfolding of the Pham singularity $-y^n + x^s = 0$ with co-prime n and s , $n < s$. Thus, an (n, s) -curve \mathcal{C} is defined by

$$(1a) \quad \mathcal{C} = \{(x, y) \in \mathbb{C}^2 \mid f(x, y) = 0\},$$

$$(1b) \quad f(x, y) \equiv -y^n + x^s + \sum_{j=0}^{n-2} \sum_{i=0}^{s-2} \lambda_{ns-in-j} y^j x^i,$$

$$(1c) \quad \lambda_{k \leq 0} = 0, \quad \lambda_k \in \mathbb{C}.$$

where λ_k serve as parameters of the curve, and k shows the Sato weight of λ_k . Only parameters with positive weights are allowed. The Sato weights of x and y are $\text{wgt } x = n$, and $\text{wgt } y = s$. Then $\text{wgt } f(x, y) = ns$. Note, that some terms are omitted in (1), since the definition contains the minimal number of parameters. All extra terms can be eliminated by a proper bi-rational transformation.

Due to n and s are co-prime, infinity is a Weierstrass point, and a branch point where all n sheets of the curve wind. Let ξ denote a local parameter near infinity, then

$$(2) \quad x = \xi^{-n}, \quad y = \xi^{-s}(1 + O(\lambda))$$

gives the simplest parametrization of (1). Evidently, the Sato weight equals the negative exponent of the leading term in the expansion near infinity.

2.2. Abel map. Let $du = (du_{\mathfrak{w}_1}, du_{\mathfrak{w}_2}, \dots, du_{\mathfrak{w}_g})^t$ be not normalized first kind differentials, labeled by elements of the Weierstrass gap sequence $\mathfrak{W} = \{\mathfrak{w}_1, \mathfrak{w}_2, \dots, \mathfrak{w}_g\}$, which coincide with negative weights of the differentials: $\text{wgt } du_{\mathfrak{w}_i} = -\mathfrak{w}_i$, and show the orders of zero at infinity.

Let the Abel map \mathcal{A} be constructed with not normalized differentials du :

$$(3) \quad \mathcal{A}(P) = \int_{\infty}^P du, \quad P = (x, y) \in \mathcal{C}.$$

Here infinity is used as the base-point, which is the standard choice in the case of (n, s) -curves.

First kind integrals along canonical homology cycles $\{\mathbf{a}_i, \mathbf{b}_i\}_{i=1}^g$ give first kind period matrices:

$$(4) \quad \omega = (\omega_{ij}) = \left(\int_{\mathbf{a}_j} du_i \right), \quad \omega' = (\omega'_{ij}) = \left(\int_{\mathbf{b}_j} du_i \right).$$

Columns of ω, ω' generate the lattice $\{\omega, \omega'\}$ of periods. Then $\text{Jac}(\mathcal{C}) = \mathbb{C}^g \setminus \{\omega, \omega'\}$ is the Jacobian variety of the curve \mathcal{C} , equipped with not normalized coordinates $u = (u_{\mathfrak{w}_1}, u_{\mathfrak{w}_2}, \dots, u_{\mathfrak{w}_g})^t$. The coordinates are labeled by elements of the Weierstrass gap sequence, and $\text{wgt } u_{\mathfrak{w}_i} = -\mathfrak{w}_i$.

Let $v = \omega^{-1}u$ be normalized coordinates on the Jacobian variety, and $(1_g, \tau)$ be normalized periods, where 1_g denotes the identity matrix of order g , and $\tau = \omega^{-1}\omega'$. Matrix τ is symmetric with a positive imaginary part: $\tau^t = \tau$, $\text{Im } \tau > 0$, that is τ belongs to the Siegel upper half-space. The Sato weight is not associated with normalized coordinates. The normalised first kind differentials are defined by

$$dv = \omega^{-1}du,$$

and the Abel map $\bar{\mathcal{A}}$ with respect to the normalized differentials is

$$(5) \quad \bar{\mathcal{A}}(P) = \int_{\infty}^P dv, \quad P = (x, y) \in \mathcal{C}.$$

2.3. Theta and sigma functions. Recall the two entire functions on $\mathbb{C}^g \supset \text{Jac}(\mathcal{C})$, which generate multiply periodic (or abelian) functions, and so serve for uniformization of a curve \mathcal{C} .

The Riemann *theta function* (or θ -function)

$$(6) \quad \theta(v; \tau) = \sum_{n \in \mathbb{Z}^g} \exp(i\pi n^t \tau n + 2i\pi n^t v)$$

is defined in terms of normalized coordinates v , and normalized period matrix τ . Theta function with characteristic is defined by

$$(7) \quad \theta[\varepsilon](v; \tau) = \exp\left(i\pi\left(\frac{1}{2}\varepsilon'^t\right)\tau\left(\frac{1}{2}\varepsilon'\right) + 2i\pi\left(v + \frac{1}{2}\varepsilon\right)^t\left(\frac{1}{2}\varepsilon'\right)\right)\theta\left(v + \frac{1}{2}\varepsilon + \tau\left(\frac{1}{2}\varepsilon'\right); \tau\right),$$

where a characteristic is a $2 \times g$ matrix $[\varepsilon] = (\varepsilon', \varepsilon)^t$ with real values within the interval $[0, 2)$. Every point u in the fundamental domain of $\text{Jac}(\mathcal{C})$ can be represented by its characteristic $[\varepsilon]$, namely

$$u = \frac{1}{2}\omega\varepsilon + \frac{1}{2}\omega'\varepsilon'.$$

In the hyperelliptic case, the Abel images of branch points, and any combination of branch points are described by characteristics with components 1 or 0, which are called half-integer characteristics. Such a characteristic is odd whenever $\varepsilon^t\varepsilon' = 0 \pmod{2}$, and even whenever $\varepsilon^t\varepsilon' = 1 \pmod{2}$. θ -Function with half-integer characteristic has the same parity as its characteristic.

The entire function on $\mathbb{C}^g \supset \text{Jac}(\mathcal{C})$ covariant under integer shifts on the period lattice is called the *sigma function* (or σ -function), see [3, p. 97]. As a definition we use its relation with θ -function, see [10, Eq.(2.3)]:

$$(8) \quad \sigma(u) = C \exp\left(-\frac{1}{2}u^t \varkappa u\right)\theta[K](\omega^{-1}u; \omega^{-1}\omega'),$$

where $[K]$ denotes the characteristic of the vector of Riemann constants, and a symmetric matrix $\varkappa = \eta\omega^{-1}$ is obtained from the second kind period matrix η . The Sato weight of σ -function is $\text{wgt } \sigma = -(n^2 - 1)(s^2 - 1)/24$, see [9].

σ -Function is defined in terms of not normalized coordinates u , and not normalized period matrices of the first kind ω , ω' , and the second kind η , η' . The latter are defined as follows

$$(9) \quad \eta = (\eta_{ij}) = \left(\int_{\mathbf{a}_j} dr_i \right), \quad \eta' = (\eta'_{ij}) = \left(\int_{\mathbf{b}_j} dr_i \right),$$

with second kind differentials $dr = (dr_{\mathbf{w}_1}, dr_{\mathbf{w}_2}, \dots, dr_{\mathbf{w}_g})^t$. It is important to choose the second kind differentials which form an associated system with differentials of the first kind, see [2, § 138]. Note that $dr_{\mathbf{w}_i}$ has the only pole of order \mathbf{w}_i at infinity, and so $\text{wgt } r_{\mathbf{w}_i} = \mathbf{w}_i$. In the vicinity of infinity, with a local parameter ξ such that $\xi(\infty) = 0$, the following relation holds

$$(10) \quad \text{res}_{\xi=0} \left(\int_0^\xi du(\tilde{\xi}) \right) dr(\xi)^t = 1_g,$$

which completely determines the principle part of $dr(\xi)$.

The not normalized period matrices of the first ω , ω' and second η , η' kinds satisfy the Legendre relation, see [2, § 140],

$$(11) \quad \Omega^t J \Omega = 2\pi i J,$$

$$\Omega = \begin{pmatrix} \omega & \omega' \\ \eta & \eta' \end{pmatrix}, \quad J = \begin{pmatrix} 0 & -1_g \\ 1_g & 0 \end{pmatrix}.$$

Multiply periodic \wp -functions are defined with the help of σ -function:

$$\wp_{i,j}(u) = -\frac{\partial^2 \log \sigma(u)}{\partial u_i \partial u_j}, \quad \wp_{i,j,k}(u) = -\frac{\partial^3 \log \sigma(u)}{\partial u_i \partial u_j \partial u_k}, \quad \text{etc.}$$

Since σ -function vanishes on special divisors according to the Riemann vanishing theorem, \wp -functions are defined on $\text{Jac}(\mathcal{C}) \setminus \Sigma$, where $\Sigma = \{u \mid \sigma(u) = 0\}$.

From (8) we obtain expressions for \wp -functions in terms of θ -function:

$$(12) \quad \wp_{i,j}(u) = \varkappa_{i,j} - \frac{\partial^2}{\partial u_i \partial u_j} \log \theta[K](\omega^{-1}u; \omega^{-1}\omega'),$$

$$\wp_{i,j,k}(u) = -\frac{\partial^3}{\partial u_i \partial u_j \partial u_k} \log \theta[K](\omega^{-1}u; \omega^{-1}\omega').$$

The vector of Riemann constants K with respect to a base-point P_0 is defined by the formula, [14, Eq. (2.4.14)]

$$(13) \quad K_j = \frac{1}{2}(1 + \tau_{j,j}) - \sum_{l \neq j} \oint_{\mathbf{a}_l} dv_j(P) \int_{P_0}^P dv_l, \quad j = 1, \dots, g.$$

In the hyperelliptic case, the vector is computed² in [16, p. 14], and equals the sum of all odd characteristics of the fundamental set of $2g + 1$ characteristics which represent branch points, according to [2, § 200–202].

²Below, we use a homology basis different from [16], and so $[K]$ is not exactly the same, but computed in the same way.

2.4. Bolza formulas and generalizations. In genus 2, expressions for branch points in terms of θ -function are known as the Bolza formulas

$$e_\iota = -\frac{\partial_{u_3}\theta[\{\iota\}](\omega^{-1}u)}{\partial_{u_1}\theta[\{\iota\}](\omega^{-1}u)}\Big|_{u=0},$$

where $[\{\iota\}]$ denotes the characteristic corresponding to a branch point e_ι , see [8, Eq. (6)]. A generalization of the Bolza formulas for a hyperelliptic curve of arbitrary genus g is obtained in [5]. In particular,

$$e_\iota = -\frac{\partial_{u_{2(g \bmod 2)+1}, \dots, u_{2g-7}, u_{2g-1}}^{[g/2]}\theta[\{\iota\}](\omega^{-1}u)}{\partial_{u_{2(g \bmod 2)+1}, \dots, u_{2g-7}, u_{2g-3}}^{[g/2]}\theta[\{\iota\}](\omega^{-1}u)}\Big|_{u=0}.$$

2.5. Jacobi inversion problem. Given a point u of the Jacobian variety $\text{Jac}(\mathcal{C})$ find a reduced divisor $D \in \mathcal{C}^g$ such that $\mathcal{A}(D) = u$. Every class of linearly equivalent divisors on a curve of genus g has a representative called a reduced divisor, let it be a positive divisor of degree g or less. Reduced divisors of degree less than g are special, and $\theta[K]$ vanishes on such divisors, according to the Riemann vanishing theorem. Reduced divisors of degree g are non-special. Every non-special divisor represents its class uniquely. The Abel image of the subspace of non-special divisors coincides with $\text{Jac}(\mathcal{C}) \setminus \Sigma$.

A solution of the Jacobi inversion problem is known for non-special divisors. On hyperelliptic curves such a solution was given in [2, § 216] and rediscovered in [10, Theorem 2.2]. Let a non-degenerate hyperelliptic curve of genus g be defined³ by

$$(14) \quad -y^2 + x^{2g+1} + \sum_{i=1}^{2g} \lambda_{2i+2} x^{2g-i} = 0.$$

Let $u = \mathcal{A}(D)$ be the Abel image of a degree g positive non-special divisor D on the curve. Then D is uniquely defined by the system of equations

$$(15a) \quad \mathcal{R}_{2g}(x; u) \equiv x^g - \sum_{i=1}^g x^{g-i} \wp_{1,2i-1}(u) = 0,$$

$$(15b) \quad \mathcal{R}_{2g+1}(x, y; u) \equiv 2y + \sum_{i=1}^g x^{g-i} \wp_{1,1,2i-1}(u) = 0.$$

On a trigonal curve, the Jacobi inversion problem is solved in [11]. A method of obtaining such a solution on a curve of an arbitrary gonality is presented in [7]; trigonal, tetragonal and pentagonal curves are considered as an illustration. In the case of a $(3, 3m+1)$ -curve, a degree g positive non-special divisor D such that $u = \mathcal{A}(D)$ is given by the system

$$(16a) \quad \mathcal{R}_{6m}(x, y; u) \equiv x^{2m} - y \sum_{i=1}^m \wp_{1,3i-2}(u) x^{m-i} - \sum_{i=1}^{2m} \wp_{1,3i-1}(u) x^{2m-i} = 0,$$

$$(16b) \quad \mathcal{R}_{6m+1}(x, y; u) \equiv 2yx^m + y \sum_{i=1}^m (\wp_{1,1,3i-2}(u) - \wp_{2,3i-2}(u)) x^{m-i} \\ + \sum_{i=1}^{2m} (\wp_{1,1,3i-1}(u) - \wp_{2,3i-1}(u)) x^{2m-i} = 0.$$

³A $(2, 2g+1)$ -curve serves as a canonical form of hyperelliptic curves of genus g .

In the case of a $(3, 3m + 2)$ -curve, by the system

(17a)

$$\mathcal{R}_{6m+2}(x, y; u) \equiv yx^m - y \sum_{i=1}^m \wp_{1,3i-1}(u)x^{m-i} - \sum_{i=1}^{2m+1} \wp_{1,3i-2}(u)x^{2m+1-i} = 0,$$

(17b)

$$\begin{aligned} \mathcal{R}_{6m+3}(x, y; u) \equiv & 2x^{2m+1} + y \sum_{i=1}^m (\wp_{1,1,3i-1}(u) - \wp_{2,3i-1}(u))x^{m-i} \\ & - \sum_{i=1}^{2m+1} (\wp_{1,1,3i-2}(u) - \wp_{2,3i-2}(u))x^{2m+1-i} = 0. \end{aligned}$$

3. PERIODS ON A HYPERELLIPTIC CURVE

Hyperelliptic curves are the best known plane algebraic curves. There exists a universal approach to choosing a homology and cohomology bases on such curves, as well as constructing the corresponding Riemann surfaces.

3.1. Hyperelliptic curves. Let a generic hyperelliptic curve be defined by

$$(18) \quad 0 = \tilde{f}(x, y) \equiv -y^2 + y\mathcal{Q}(x) + \mathcal{P}(x),$$

where $\deg \mathcal{P} = 2g + 1$ or $2g + 2$, in the case of genus g .

An equation with $\deg \mathcal{P} = 2g + 1$, $\mathcal{Q}(x) \equiv 0$ defines an (n, s) -curve, which is considered as the canonical form of a hyperelliptic curve of genus g :

$$(19) \quad 0 = f(x, y) \equiv -y^2 + x^{2g+1} + \lambda_4 x^{2g-1} + \cdots + \lambda_{4g} x + \lambda_{4g+2}.$$

The Sato weights are $\text{wgt } x = 2$, $\text{wgt } y = 2g + 1$, and so $\text{wgt } f = 4g + 2$.

The term $y\mathcal{Q}(x)$ in (18) is eliminated by the map $y \mapsto \tilde{y} + \frac{1}{2}\mathcal{Q}(x)$, which leads to

$$0 = \tilde{f}(x, \tilde{y}) \equiv -\tilde{y}^2 + \tilde{\mathcal{P}}(x), \quad \tilde{\mathcal{P}}(x) = \mathcal{P}(x) + \frac{1}{4}\mathcal{Q}(x)^2.$$

Thus, the discriminant of (18) is defined by the formula

$$(20) \quad \Delta(x) = \tilde{\mathcal{P}}(x) = \mathcal{P}(x) + \frac{1}{4}\mathcal{Q}(x)^2.$$

A canonical curve can be defined by its branch points $\{(e_i, 0)\}_{i=1}^{2g+1}$, namely

$$(21) \quad 0 = f(x, y) = -y^2 + \mathcal{P}(x), \quad \mathcal{P}(x) = \prod_{j=1}^{2g+1} (x - e_j).$$

For the sake of brevity, the notation e_i is employed both for a branch point $(e_i, 0)$ and its x -coordinate, in the hyperelliptic case. If all branch points are distinct, then the curve is non-degenerate, and its genus equals g . The curve (21) has also a branch point located at infinity, referred as e_0 . Finite branch points $\{e_i\}$ of the curve (19) satisfy the condition $\sum_{i=1}^{2g+1} e_i = 0$. Without this condition, \mathcal{P} in (21) contains also the term $\lambda_2 x^{2g}$. In what follows, we omit such a condition, and allow $\{e_i\}$ be arbitrary.

A curve with $\deg \mathcal{P} = 2g + 2$, and $\mathcal{Q}(x) \equiv 0$ has $2g + 2$ finite branch points $\{(e_i, 0)\}_{i=0}^{2g+1}$. The corresponding canonical form is obtained by moving the finite branch point e_0 to infinity by means of a proper Möbius transformation.

In the generic case (18), the maximal $\deg \mathcal{Q}$ equals g , which respects the Sato weight, and guarantees that the genus of the curve does not exceed g . Such a curve

can be defined by choosing arbitrary values $\{e_i\}$ of number $2g + 1$ or $2g + 2$, and choosing a polynomial \mathcal{Q} of a degree up to g . Then the corresponding y -coordinates of branch points $\{B_i = (e_i, h_i)\}$ are obtained by the formula $h_i = \frac{1}{2}\mathcal{Q}(e_i)$.

The Weierstrass gap sequence of a hyperelliptic curve (18) is

$$\mathfrak{W} = \{\mathfrak{w}_i = 2i - 1 \mid i = 1, \dots, g\}.$$

In what follows, we focus on the form (21) of a hyperelliptic curve.

3.2. Riemann surface. At every point x , except branch points, there exist two values of y ($s = \pm 1$):

$$(22a) \quad y_s(x) = s\sqrt{\Delta(x)}, \quad \Delta(x) = \mathcal{P}(x), \quad \text{in the canonical case,} \quad \text{or}$$

$$(22b) \quad y_s(x) = \frac{1}{2}\mathcal{Q}(x) + s\sqrt{\Delta(x)}, \quad \text{in the generic case.}$$

Let the square root function be defined as follows

$$(23) \quad \sqrt{\Delta(x)} = \begin{cases} \sqrt{|\Delta(x)|} e^{(i/2)\arg \Delta(x)} & \text{if } \arg \Delta(x) \geq 0, \\ \sqrt{|\Delta(x)|} e^{(i/2)\arg \Delta(x) + i\pi} & \text{if } \arg \Delta(x) < 0, \end{cases}$$

where \arg has the range $(-\pi, \pi]$. With such a definition the range of $\arg \sqrt{\Delta(x)}$ is $[0, \pi)$. Moreover,

Theorem 1. *Let $\sqrt{\Delta}$ be defined by (23). Then y_s defined by (22) have discontinuity over the contour $\Gamma = \{x \mid \arg \Delta(x) = 0\}$, and y_+ serves as the analytic continuation of y_- on the other side of the contour, and vice versa.*

Proof. Let \tilde{x} be located in the vicinity of the contour Γ , more precisely $|\arg \Delta(\tilde{x})| < 2\phi$, with a small positive value ϕ . Then $0 \leq \arg \sqrt{\Delta(\tilde{x})} < \phi$ if $\arg \Delta(\tilde{x}) \geq 0$, and $\pi - \phi < \arg \sqrt{\Delta(\tilde{x})} < \pi$ if $\arg \Delta(\tilde{x}) < 0$. Evidently, the discontinuity of $\sqrt{\Delta}$ is located over the contour Γ .

Next, we find the analytic continuation of $\sqrt{\Delta}$. Let $U(x_0; \delta)$ be a disc of radius δ with the center at $x_0 \in \Gamma$. The contour Γ divides the disc into two parts: U_+ where $\arg \Delta(x) \geq 0$, and U_- where $\arg \Delta(x) < 0$. Let $2\phi_+ = \max_{\tilde{x} \in U_+} \arg \Delta(\tilde{x})$, then the range of $\arg \sqrt{\Delta}$ on U_+ is $[0, \phi_+)$. Let $-2\phi_- = \min_{\tilde{x} \in U_-} \arg \Delta(\tilde{x})$, then the range of $\arg \sqrt{\Delta}$ on U_- is $(\pi - \phi_-, \pi)$. Thus, the analytic continuation of $\sqrt{\Delta}$ from U_+ to U_- is $-\sqrt{\Delta}$, since the range of $\arg(-\sqrt{\Delta(\tilde{x})}) = \arg(e^{-i\pi} \sqrt{\Delta(\tilde{x})})$ on U_- is $(-\phi_-, 0)$. And the analytic continuation of $\sqrt{\Delta}$ from U_- to U_+ is given by $-\sqrt{\Delta} = e^{i\pi} \sqrt{\Delta}$, with the range $[\pi, \pi + \phi_+)$ of $\arg(-\sqrt{\Delta})$ on U_+ . \square

With the help of definition (23), we fix the position of discontinuity of $\sqrt{\Delta}$ at the contour Γ . This allows to determine connection of solutions y_s on the Riemann surface, and mark sheets.

In order to construct the Riemann surface of a curve, we choose a continuous path γ on the Riemann sphere through all $\{e_i\}$, starting and ending at $e_0 = \infty$. Along γ , at any intersection with Γ the sign s in (22) changes into the opposite. Thus, sequences of signs along γ lifted to each sheet mark the sheets. And so the *monodromy* of the Riemann surface is defined, cf. [13, Sect. 2.7]. We call γ the *monodromy path*.

3.3. Monodromy path. The monodromy path γ is the *key element* of the proposed scheme of constructing an analytical model of the Riemann surface of \mathcal{C} .

The path starts at infinity as $x \rightarrow -\infty$, goes through all branch points in a chosen order, and ends at infinity as $x \rightarrow \infty$. Below, an algorithm of drawing such a path and marking sheets is presented.

1. Let all finite branch points $\{e_i\}_{i=1}^{2g+1}$ be sorted ascendingly first by the real part, then by the imaginary part.
2. According to this order a continuous path γ through all e_i is constructed from straight line segments $[e_i, e_{i+1}]$, $i = 1, \dots, 2g$. Then the segment $(-\infty, e_1]$ is added at the beginning of the polygonal path, and $[e_{2g+1}, \infty)$ at the end. The path goes below the points $\{e_i\}$, and so in the counter-clockwise direction near each e_i . Such a path is marked in orange on fig. 2.
3. Plot the contour $\Gamma = \{x \mid \arg \mathcal{P}(x) = 0\}$, which consists of segments Γ_i between e_i and infinity, see blue contours on fig. 2. Find the sequence of signs $\{\mathfrak{s}_{0,1}\} \cup \{\mathfrak{s}_{i,i+1}\}_{i=1}^{2g} \cup \{\mathfrak{s}_{2g+1,0}\}$ corresponding to the sequence of segments of the path γ , starting with $\mathfrak{s}_{0,1} = +1$. Index 0 is used for infinity. At any intersection with Γ the sign changes into the opposite. The sequence of signs determines connection between solutions y_s on Sheet **a**. Sheet **b** is marked by the sequence with the opposite sign on each segment. On a hyperelliptic curve, Sheet **a** is sufficient for all computations.

Remark 1. It could happen, that an intersection of a polygonal path γ with Γ is caused by curling of Γ around a branch point. Such an intersection could be avoided by continuous deformation of γ .

3.4. Homology. Cuts are made between points e_{2k-1} and e_{2k} with k from 1 to g , and from e_{2g+1} to infinity. With k running from 1 to g an \mathfrak{a}_k -cycle encircles the cut (e_{2k-1}, e_{2k}) counter-clockwise, and a \mathfrak{b}_k -cycle enters the cut (e_{2k-1}, e_{2k}) and emerges from the cut (e_{2g+1}, ∞) , see fig. 1 as an example. This canonical homology basis is adopted from Baker [2, p. 297], and can be considered as standard on a hyperelliptic curve.

Remark 2. In the case of $\deg \mathcal{P} = 2g+2$, with branch points $\{(e_i, 0)\}_{i=0}^{2g+1}$, we sort the latter in the same way as in the canonical case. So e_0 has the smallest real and imaginary parts among all branch points. Cuts are made between points e_{2k-1} and e_{2k} with k from 1 to g , and from e_{2g+1} to e_0 through infinity. A canonical homology basis is introduced in a similar way: an \mathfrak{a}_k -cycle encircles the cut (e_{2k-1}, e_{2k}) counter-clockwise, and a \mathfrak{b}_k -cycle enters the cut (e_{2k-1}, e_{2k}) and emerges from the cut $(e_{2g+1}, \infty) \cup (\infty, e_0)$.

3.5. Cohomology. First kind differentials are defined in the standard way, see [2, Ex. i, p. 195] for example,

$$(24) \quad du_{2i-1} = \frac{x^{g-i} dx}{\partial_y f(x, y)}, \quad i = 1, \dots, g.$$

On the canonical hyperelliptic curve, the second kind differentials associated with the first kind ones have the form ($\lambda_0 = 1$)

$$(25) \quad dr_{2i-1} = \frac{dx}{\partial_y f(x, y)} \sum_{k=1}^{2i-1} k \lambda_{4i-2k-2} x^{g-i+k}, \quad i = 1, \dots, g.$$

3.6. Computation of periods. First kind integrals on each segment along the polygonal monodromy path γ lifted to Sheet **a** are computed by

$$(26a) \quad \mathcal{A}_{i,i+1}^{[s_{i,i+1}]} = \int_{e_i}^{e_{i+1}} du^{[s_{i,i+1}]}, \quad i = 1, \dots, 2g,$$

$$(26b) \quad \mathcal{A}_{0,1}^{[s_{0,1}]} = \int_{-\infty}^{e_1} du^{[s_{0,1}]}, \quad \mathcal{A}_{2g+1,0}^{[s_{2g+1,0}]} = \int_{e_{2g+1}}^{\infty} du^{[s_{2g+1,0}]}.$$

The integrand of $\mathcal{A}_{i,j}^{[s_{i,j}]}$ is taken with the sign $s_{i,j}$, that is

$$du^{[s_{i,j}]} = \begin{pmatrix} x^{g-1} \\ \vdots \\ x \\ 1 \end{pmatrix} \frac{dx}{-2s_{i,j}\sqrt{\mathcal{P}(x)}}.$$

Due to the involution of a hyperelliptic curve, the following relations hold

$$(27) \quad \sum_{k=1}^g \mathcal{A}_{2k-1,2k}^{[s_{2k-1,2k}]} + \mathcal{A}_{2g+1,0}^{[s_{2g+1,0}]} = 0, \quad \mathcal{A}_{0,1}^{[s_{0,1}]} + \sum_{k=1}^g \mathcal{A}_{2k,2k+1}^{[s_{2k,2k+1}]} = 0,$$

which serve for verification.

According to the choice of canonical cycles, columns of the first kind period matrices are

$$(28) \quad \omega_k = 2\mathcal{A}_{2k-1,2k}^{[s_{2k-1,2k}]}, \quad \omega'_k = -2 \sum_{j=k}^g \mathcal{A}_{2j,2j+1}^{[s_{2j,2j+1}]}.$$

The normalized period matrix, which is the Riemann period matrix, is obtain by

$$\tau = \omega^{-1}\omega',$$

and required to be symmetric with a positive imaginary part.

Second kind integrals $\mathcal{B}_{i,j}^{[s_{i,j}]}$ are computed similarly:

$$\mathcal{B}_{i,j}^{[s_{i,j}]} = \int_{e_i}^{e_j} dr^{[s_{i,j}]},$$

where $dr^{[s_{i,j}]}$, defined by (25), is taken with the sign $s_{i,j}$. Then the second kind period matrices are

$$(29) \quad \eta_k = 2\mathcal{B}_{2k-1,2k}^{[s_{2k-1,2k}]}, \quad \eta'_k = -2 \sum_{j=k}^g \mathcal{B}_{2j,2j+1}^{[s_{2j,2j+1}]}.$$

The symmetric matrix responsible for modular invariance⁴ is

$$\varkappa = \eta\omega^{-1}.$$

The four matrices $\omega, \omega', \eta, \eta'$ satisfy the Legendre relation (11), which serve for verification.

⁴By introducing the exponential factor with \varkappa , the theta function is transformed into the modular invariant sigma function, cf. (8).

3.7. Example 1: Arbitrary complex branch points. Let a hyperelliptic curve of genus 4 possess the given finite branch points:

$$-18 - 2i, -16 + 5i, -11 + 3i, -10 - i, -4 + 2i, -3 + 3i, 3 + 3i, 7 - 2i, 13 - i.$$

On the other hand, this curve is defined by the equation

$$(30a) \quad 0 = f(x, y) \equiv -y^2 + \mathcal{P}(x),$$

$$(30b) \quad \begin{aligned} \mathcal{P}(x) = & x^9 + (39 - 10i)x^8 + (217 - 288i)x^7 - (7585 - 826i)x^6 \\ & - (79138 - 82462i)x^5 + (324058 + 455846i)x^4 + (4126332 - 3930980i)x^3 \\ & - (14219032 + 29444932i)x^2 - (131012592 - 28208616i)x \\ & - 101860560 + 245519280i. \end{aligned}$$

Cuts and homology cycles, see fig.1, are introduced as explained in subsection 3.4. On fig. 2, the contour Γ is shown in blue. Note, that the cut (e_9, ∞)

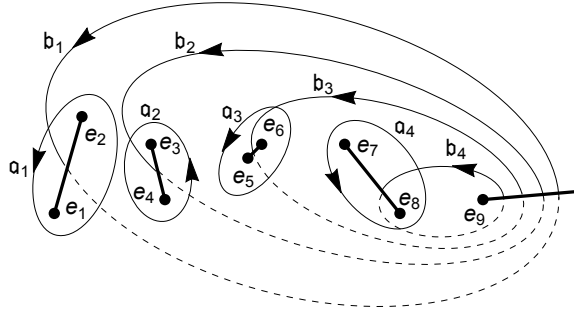


FIGURE 1. Canonical homology cycles.

coincides with segment Γ_9 . The monodromy path γ is marked in orange. It goes below points e_i . A curved orange line near a cut shows on which side of the cut γ goes.

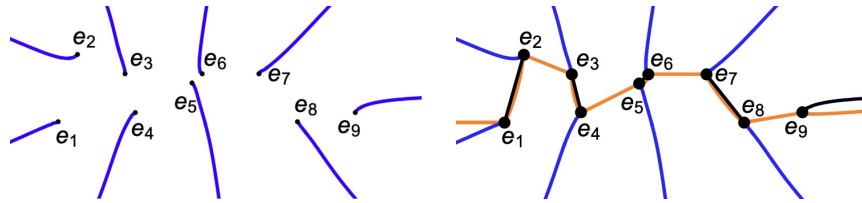
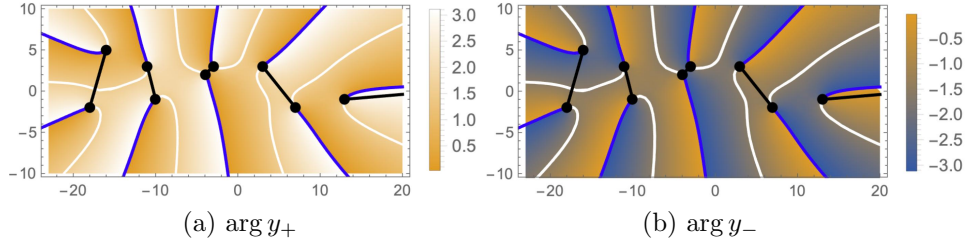
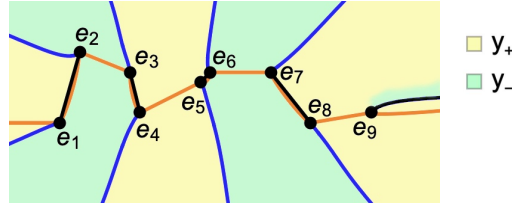


FIGURE 2. The contour Γ (blue), and a continuous path (orange).

As seen on fig. 3, along the contour Γ solution y_+ continuously connects to y_- , and vice versa.

Now we mark Sheet a, see fig. 4. Let start with $s_{0,1} = +1$ on segment $(-\infty, e_1]$. The path γ (orange) intersects the blue contour at point e_1 , and so the sign changes: $s_{1,2} = -1$. The path goes along the right side of the cut (e_1, e_2) , and the sign remains the same on the next segment: $s_{2,3} = -1$. From e_3 to e_4 the path goes along the left side of the cut (e_3, e_4) , so the sign remains the same: $s_{3,4} = -1$. The next intersection with the blue contour occurs at point e_4 , thus $s_{4,5} = +1$. And

FIGURE 3. Density plots of $\arg y_s$, and the contour Γ (blue).FIGURE 4. Connection of solutions y_+ and y_- on Sheet a.

again at point e_5 , so $s_{5,6} = s_{6,7} = s_{7,8} = -1$. Once again, the path γ intersects the blue contour at point e_8 , thus $s_{8,9} = s_{9,0} = +1$. Finally, the sequence of signs is

$$\{s_{0,1}, s_{1,2}, s_{2,3}, s_{3,4}, s_{4,5}, s_{5,6}, s_{6,7}, s_{7,8}, s_{8,9}, s_{9,0}\} =$$

Sheet a: $\{+1, -1, -1, -1, +1, -1, -1, -1, +1, +1\}$.

Along segment Γ_9 solution y_+ on Sheet a connects to y_- on Sheet b, the latter is shown in green above of Γ_9 , see fig. 4.

First kind differentials as functions of x are

$$du^{[s]} = \begin{pmatrix} x^3 \\ x^2 \\ x \\ 1 \end{pmatrix} \frac{dx}{-2s\sqrt{\mathcal{P}(x)}}.$$

According to the picture of homology cycles, see fig.1, the first kind period matrices ω and ω' are computed as follows, cf. (28),

$$\omega = 2(\mathcal{A}_{1,2}^{[-]}, \mathcal{A}_{3,4}^{[-]}, \mathcal{A}_{5,6}^{[-]}, \mathcal{A}_{7,8}^{[-]}),$$

$$\omega' = -2(\mathcal{A}_{2,3}^{[-]} + \mathcal{A}_{4,5}^{[+]} + \mathcal{A}_{6,7}^{[-]} + \mathcal{A}_{8,9}^{[+]}, \mathcal{A}_{4,5}^{[-]} + \mathcal{A}_{6,7}^{[+]} + \mathcal{A}_{8,9}^{[-]}, \mathcal{A}_{6,7}^{[-]} + \mathcal{A}_{8,9}^{[+]}).$$

Numerical computation of $\mathcal{A}_{i,j}^{[s_i,j]}$ is performed with the help of function `NIntegrate` with a `WorkingPrecision` of 18. The relations (27) are satisfied with an accuracy of 10^{-16} . On the curve (30) we obtain

$$\omega \approx \begin{pmatrix} -1.303573 + 0.207439i & 0.848115 - 0.306788i \\ 0.073367 - 0.003075i & -0.083799 + 0.019801i \\ -0.003985 - 0.000333i & 0.008037 - 0.001042i \\ 0.000208 + 0.000046i & -0.000751 + 0.000028i \end{pmatrix}$$

$$\omega' \approx \begin{pmatrix} 0.0166625 + 0.063503\iota & -0.035439 - 0.017840\iota \\ 0.005372 - 0.014707\iota & -0.007363 - 0.005200\iota \\ -0.003023 + 0.002108\iota & -0.001651 - 0.000958\iota \\ 0.000856 + 0.000006\iota & -0.000350 - 0.000098\iota \end{pmatrix},$$

$$\approx \begin{pmatrix} -0.604960 - 0.930374\iota & -0.085127 + 0.237963\iota \\ 0.029948 + 0.024444\iota & 0.019758 - 0.067832\iota \\ -0.001525 - 0.000835\iota & -0.002854 + 0.005901\iota \\ 0.000078 + 0.000029\iota & 0.000324 - 0.000426\iota \end{pmatrix}$$

$$\approx \begin{pmatrix} 0.042341 - 0.110642\iota & 0.047121 - 0.129831\iota \\ 0.011312 - 0.018512\iota & 0.006638 - 0.011849\iota \\ -0.002257 - 0.001647\iota & 0.000894 - 0.001058\iota \\ 0.000178 + 0.000796\iota & 0.000117 - 0.000089\iota \end{pmatrix}.$$

The corresponding normalized period matrix from the Siegel upper half-space is

$$\tau \approx \begin{pmatrix} 0.416960 + 1.348235\iota & -0.019631 + 0.866637\iota \\ -0.019631 + 0.866637\iota & -0.401986 + 1.468494\iota \\ 0.043442 + 0.592788\iota & 0.090347 + 0.771653\iota \\ 0.013536 + 0.360353\iota & 0.020075 + 0.430424\iota \end{pmatrix}$$

$$\approx \begin{pmatrix} 0.043442 + 0.592788\iota & 0.013536 + 0.360353\iota \\ 0.090347 + 0.771653\iota & 0.020075 + 0.430424\iota \\ 0.276110 + 1.677311\iota & -0.019449 + 0.549477\iota \\ -0.019449 + 0.549477\iota & -0.241045 + 0.959518\iota \end{pmatrix}.$$

The symmetric property of τ is satisfied with an accuracy of 10^{-15} .

With the second kind differentials

$$(31) \quad dr_{2i-1}^{[s]} = \frac{R_{2i-1}(x) dx}{-2s \sqrt{\mathcal{P}(x)}}, \quad i = 1, 2, 3, 4,$$

$$R_1 = x^4,$$

$$R_3 = 3x^5 + (78 - 20\iota)x^4 + (217 - 288\iota)x^3,$$

$$R_5 = 5x^6 + (156 - 40\iota)x^5 + (651 - 864\iota)x^4 - (15170 - 1652\iota)x^3$$

$$- (79138 - 82462\iota)x^2,$$

$$R_7 = 7x^7 + (234 - 60\iota)x^6 + (1085 - 1440\iota)x^5 - (30340 - 3304\iota)x^4$$

$$- (237414 - 247386\iota)x^3 + (648116 + 911692\iota)x^2$$

$$+ (4126332 - 3930980\iota)x,$$

second kind periods are computed:

$$\eta \approx \begin{pmatrix} 22.428062 - 6.098673\iota & -8.281570 + 4.260894\iota \\ 280.811215 - 73.921437\iota & -233.173130 + 22.293105\iota \\ 910.855655 + 10.721526\iota & -2603.233939 - 813.570166\iota \\ 1224.707652 + 409.922637\iota & -7484.857429 - 1328.792554\iota \end{pmatrix}$$

$$\approx \begin{pmatrix} -0.205360 - 0.177582\iota & -0.198185 - 0.006055\iota \\ 5.630286 - 0.370818\iota & -32.028810 + 11.479858\iota \\ 299.647570 + 719.376216\iota & 1242.433044 + 350.238889\iota \\ 487.787097 + 8861.332415\iota & 6189.443173 - 7889.884228\iota \end{pmatrix},$$

$$\eta' \approx \begin{pmatrix} 13.855811 + 9.185567\iota & 1.880170 - 4.181065\iota \\ 150.913701 + 40.841618\iota & 64.433701 - 272.113911\iota \\ 420.612695 + 72.624802\iota & 1188.248232 - 1359.820959\iota \\ 504.296929 + 98.209496\iota & 3559.979547 - 2711.948811\iota \\ 0.264151 - 1.540944\iota & 0.305811 - 1.421979\iota \\ -26.525723 - 208.762530\iota & -27.152420 - 206.017\iota \\ -1290.627353 - 496.867943\iota & -1470.266735 - 1061.435845\iota \\ -9584.859568 + 9412.897457\iota & -2002.776466 + 2196.979511\iota \end{pmatrix},$$

and the matrix

$$\varkappa \approx \begin{pmatrix} -26.150273 + 5.226639\iota & -113.639362 + 91.745099\iota \\ -113.639362 + 91.745099\iota & 2527.918193 + 333.2000001\iota \\ 815.048336 + 59.142845\iota & 6691.213749 - 15142.962600\iota \\ 2796.548807 - 2715.208601\iota & -19805.451622 - 22245.716646\iota \\ 815.048336 + 59.142845\iota & 2796.548807 - 2715.208601\iota \\ 6691.213749 - 15142.962600\iota & -19805.451622 - 22245.716646\iota \\ -501204.576087 - 151451.871496\iota & -1572965.591976 + 1699015.043174\iota \\ -1572965.591976 + 1699015.043174\iota & -403196.119224 + 19865411.502694\iota \end{pmatrix}.$$

The symmetric property of \varkappa is accurate up to 10^{-8} , and the Legendre relation up to 10^{-14} .

Verification. An analog of the Bolza formulas on a genus 4 hyperelliptic curve, see [5, Eq. (40)], is given by

$$(32) \quad e_\iota = -\frac{\partial_{u_1, u_7}^2 \theta[\{\iota\}](\omega^{-1}u)}{\partial_{u_1, u_5}^2 \theta[\{\iota\}](\omega^{-1}u)} \Big|_{u=0}.$$

According to the chosen homology basis, we have the following correspondence between characteristics and branch points:

$$\begin{array}{lll} e_1 = -18 - 2\iota & [\varepsilon_1] = \begin{pmatrix} 1 & 0 & 0 & 0 \\ 0 & 0 & 0 & 0 \end{pmatrix} & [\{1\}] = \begin{pmatrix} 0 & 1 & 1 & 1 \\ 0 & 1 & 0 & 1 \end{pmatrix}, \\ e_2 = -16 + 5\iota & [\varepsilon_2] = \begin{pmatrix} 1 & 0 & 0 & 0 \\ 1 & 0 & 0 & 0 \end{pmatrix} & [\{2\}] = \begin{pmatrix} 0 & 1 & 1 & 1 \\ 1 & 1 & 0 & 1 \end{pmatrix}, \\ e_3 = -11 + 3\iota & [\varepsilon_3] = \begin{pmatrix} 0 & 1 & 0 & 0 \\ 1 & 0 & 0 & 0 \end{pmatrix} & [\{3\}] = \begin{pmatrix} 1 & 0 & 1 & 1 \\ 1 & 1 & 0 & 1 \end{pmatrix}, \\ e_4 = -10 - \iota & [\varepsilon_4] = \begin{pmatrix} 0 & 1 & 0 & 0 \\ 1 & 1 & 0 & 0 \end{pmatrix} & [\{4\}] = \begin{pmatrix} 1 & 0 & 1 & 1 \\ 1 & 0 & 0 & 1 \end{pmatrix}, \\ e_5 = -4 + 2\iota & [\varepsilon_5] = \begin{pmatrix} 0 & 0 & 1 & 0 \\ 1 & 1 & 0 & 0 \end{pmatrix} & [\{5\}] = \begin{pmatrix} 1 & 1 & 0 & 1 \\ 1 & 0 & 0 & 1 \end{pmatrix}, \\ e_6 = -3 + 3\iota & [\varepsilon_6] = \begin{pmatrix} 0 & 0 & 1 & 0 \\ 1 & 1 & 1 & 0 \end{pmatrix} & [\{6\}] = \begin{pmatrix} 1 & 1 & 0 & 1 \\ 1 & 0 & 1 & 1 \end{pmatrix}, \\ e_7 = 3 + 3\iota & [\varepsilon_7] = \begin{pmatrix} 0 & 0 & 0 & 1 \\ 1 & 1 & 1 & 0 \end{pmatrix} & [\{7\}] = \begin{pmatrix} 1 & 1 & 1 & 0 \\ 1 & 0 & 1 & 1 \end{pmatrix}, \\ e_8 = 7 - 2\iota & [\varepsilon_8] = \begin{pmatrix} 0 & 0 & 0 & 1 \\ 1 & 1 & 1 & 1 \end{pmatrix} & [\{8\}] = \begin{pmatrix} 1 & 1 & 1 & 0 \\ 1 & 0 & 1 & 0 \end{pmatrix}, \end{array}$$

$$e_9 = 13 - \iota \quad [\varepsilon_9] = \begin{pmatrix} 0 & 0 & 0 & 0 \\ 1 & 1 & 1 & 1 \end{pmatrix} \quad [\{9\}] = \begin{pmatrix} 1 & 1 & 1 & 1 \\ 1 & 0 & 1 & 0 \end{pmatrix},$$

where $[\{\iota\}] = [\varepsilon_\iota] + [K]$, and

$$(33) \quad [K] = \sum_{i=1}^4 [\varepsilon_{2i}] = \begin{pmatrix} 1 & 1 & 1 & 1 \\ 0 & 1 & 0 & 1 \end{pmatrix}.$$

The zero matrix serves as the characteristic $[\varepsilon_0]$ of the branch point e_0 at infinity. The method of computing characteristics is adopted from [15, p. 1012].

The formulas (32) are satisfied with an accuracy of 10^{-14} .

Remark 3. Period matrices of the first kind obtained for the curve (30) with the help of `algcures` differ from the presented results, as well as a different and much more tangled homology basis is chosen for computation. The period matrices obtained from `algcures` satisfy the Bolza formulas for nine half-integer characteristics. A correspondence between characteristics and branch points is not clear from the homology basis chosen for computation, though one can discover this correspondence by applying the Bolza formulas to all characteristics.

3.8. Example 2: Real branch points. Consider briefly the case of a curve (21) with all real branch points:

$$-18, -15, -11, -5, 1, 2, 7, 12, 16.$$

Such a curve is defined by the equation

$$(34) \quad 0 = -y^2 + x^9 + 11x^8 - 514x^7 - 4602x^6 + 82441x^5 + 506395x^4 - 4495768x^3 - 11079084x^2 + 54907920x - 39916800.$$

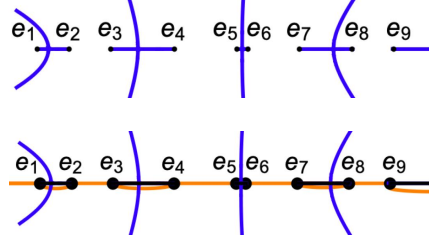


FIGURE 5. The contour Γ (blue), and a continuous path γ (orange).

The contour Γ and the monodromy path γ through all branch points are shown on fig. 5. In this case, the sequence of signs has a clear pattern:

$$\{s_{0,1}, s_{1,2}, s_{2,3}, s_{3,4}, s_{4,5}, s_{5,6}, s_{6,7}, s_{7,8}, s_{8,9}, s_{9,0}\} = \{+1, -1, -1, +1, +1, -1, -1, +1, +1, -1\}.$$

Remark 4. Note, that cuts coincide with horizontal segments of the contour Γ , and so the sign changes when the left end-point of a cut is reached, that is at every e_{2k-1} , $k = 1, \dots, g + 1$. This implies, $s_{4k-3,4k-2} = s_{4k-2,4k-1} = -1$, $k = 1, \dots, [(g+1)/2]$, and $s_{4k-1,4k} = s_{4k,4k+1} = +1$, $k = 1, \dots, [g/2]$, since we always start with $s_{0,1} = +1$. The final segment has the sign $s_{2g+1,0} = -1$ if the genus is even, or $s_{2g+1,0} = +1$ if the genus is odd.

First kind not normalized periods are

$$\omega \approx \begin{pmatrix} -0.675637 & 0.287434 & 0.002651 & -0.309937 \\ 0.041299 & -0.032471 & 0.001599 & -0.031911 \\ -0.002535 & 0.003908 & 0.001010 & -0.003404 \\ 0.000156 & -0.000507 & 0.000673 & -0.000377 \end{pmatrix},$$

$$\omega' \approx \begin{pmatrix} -0.939638i & -0.289356i & -0.312311i & -0.394964i \\ 0.030634i & -0.018895i & -0.013110i & -0.028577i \\ -0.001371i & 0.002447i & 0.001224i & -0.002089i \\ 0.000066i & -0.000232i & 0.000698i & -0.000154i \end{pmatrix}.$$

Then the normalized period matrix from the Siegel upper half-space is

$$\tau \approx \begin{pmatrix} 1.602330i & 0.820786i & 0.514534i & 0.304355i \\ 0.820786i & 1.304404i & 0.648249i & 0.359593i \\ 0.514534i & 0.648249i & 1.686169i & 0.501628i \\ 0.304355i & 0.359593i & 0.501628i & 0.948644i \end{pmatrix}.$$

Remark 5. When all branch points are real, the monodromy path γ coincides with the real axis. Moreover, \mathcal{P} is real-valued along γ , positive on segments $[e_{2k-1}, e_{2k}]$, $k = 1, \dots, g+1$, where cuts are made, and negative on the remaining segments $[e_{2k}, e_{2k+1}]$, $k = 0, \dots, g$. If one branch point of a curve is located at infinity, then e_0 stands for $-\infty$, end e_{2g+2} stands for ∞ . If all branch points are finite, then e_{2g+2} denotes the same point as e_0 , which is the smallest one.

Since \mathcal{P} has an alternating sign along the path, all \mathfrak{a} -periods are real, and all \mathfrak{b} -periods are purely imaginary. Moreover,

$$(35) \quad y(x) = (-i)^j \sqrt{|\mathcal{P}(x)|} \quad \text{on } [e_j, e_{j+1}], \quad j = 0, \dots, 2g+1.$$

The formula (35) was discovered by V. Enolsky. It shows how y_+ and y_- connect on Sheet **a**.

Second kind periods on the curve (34) computed by (31) with

$$\begin{aligned} R_1 &= x^4, \\ R_3 &= 3x^5 + 22x^4 - 514x^3, \\ R_5 &= 5x^6 + 44x^5 - 1542x^4 - 9204x^3 + 82441x^2, \\ R_7 &= 7x^7 + 66x^6 - 2570x^5 - 18408x^4 \\ &\quad + 247323x^3 + 1012790x^2 - 4495768x \end{aligned}$$

are

$$\eta \approx \begin{pmatrix} 11.099150 & -2.673068 & 0.004562 & -3.109806 \\ 42.176466 & -129.207930 & -1.238236 & -5.426458 \\ -383.268207 & -1342.343715 & 100.817590 & 1906.755187 \\ -578.759149 & 4760.249993 & -2368.318297 & -1963.133866 \end{pmatrix},$$

$$\eta' \approx \begin{pmatrix} 3.501174i & -5.136174i & -5.034880i & -5.515607i \\ -11.2650450i & -187.532997i & -174.869192i & -151.780483i \\ -195.044640i & 288.885494i & 811.312906i & 816.306629i \\ -195.450172i & 1246.674997i & 6300.606235i & -562.511001i \end{pmatrix},$$

and the symmetric matrix is

$$\varkappa \approx \begin{pmatrix} -13.123159 & 129.285113 & 1107.820797 & -1910.386399 \\ 129.285113 & 1362.173530 & -26772.601447 & 34575.690532 \\ 1107.820797 & -26772.601447 & -519356.757226 & 988034.553637 \\ -1910.386399 & 34575.690532 & 988034.553637 & -5074619.889795 \end{pmatrix}.$$

Numerical integration is performed with a `WorkingPrecision` of 18. The same accuracy as in Example 1 is achieved.

4. COMPUTATION OF \wp -FUNCTIONS ON A HYPERELLIPTIC CURVE

We start with computing the Abel image $\mathcal{A}(P)$ of a given point P by (3), where the standard not normalized holomorphic differentials (24) are used. A choice of the path from the base-point to P is tightly attached to the Riemann surface constructed in the previous section. Below, an explanation how to choose such a path correctly is given. The Abel image of a divisor $D = \sum_{i=1}^n P_i$ is computed by

$$(36) \quad \mathcal{A}(D) = \sum_{i=1}^n \mathcal{A}(P_i).$$

The Abel image of any divisor can be computed in this way.

\wp -Functions are defined on non-special divisors only. We compose non-special divisors D as positive divisors of degree $n \geq g$ with no pairs of points in involution on a hyperelliptic curve of genus g . \wp -Functions are calculated at $u = \mathcal{A}(D)$ by means of (12), where the characteristic $[K]$ of the vector of Riemann constants is required.

On a hyperelliptic curve, $[K]$ is computed as a sum of odd characteristics corresponding to branch points, cf. (33). The same $[K]$ is obtained from the formula (13). The function $\theta[K]$ has the maximal order of vanishing at $u = 0$ computed with respect to the Sato weight. The order of vanishing⁵ coincides with the negative Sato weight of σ -function, which is $-\text{wgt } \sigma = \frac{1}{2}(g+1)g$ on a hyperelliptic curve of genus g , for more details see Theorem 4 in section 6.

Let $P_i = (x_i, y_i)$. We choose e_i close to x_i , such that y_s does not change the sign over the segment $[e_i, x_i]$. The sheet where P_i is located is identified from comparing the sign n of $y_i = y_n(x_i)$ with the sign on $[e_i, x_i]$ according to the sequence of signs on Sheet a . A path to P_i is drawn on the sheet where the point is located. The path starts at $-\infty$ on the real axis, and goes to e_i along γ^n , the lift of γ on Sheet n . Then the segment $[e_i, x_i]$ on the same sheet is added to this path. Along the path to P_i the Abel image $\mathcal{A}(P_i)$ is computed.

The proposed algorithm is illustrated by examples. Divisors of degree equal to the genus g of a curve are considered, and so the Jacobi inversion problem is used for verification. One can compute \wp -functions on a divisor of degree greater than g , and solve the Jacobi inversion problem for the corresponding reduced divisor. The latter serve as an implementation of addition on a curve.

4.1. Example 1a. We continue to work with the curve (30) from Example 1 in the previous section.

⁵See computation of the order of vanishing of $\theta[K]$ with respect to not normalized coordinates in <https://community.wolfram.com/groups/-/m/t/3296279>, where $[K]$ are computed for Examples 1 and 3 from this paper.

Let u be the Abel image of a non-special divisor $D = \sum_{i=1}^4 P_i$,

$$\begin{aligned}
 P_1 &= (x_1, y_1) = (-9 + \iota, -8\sqrt{-918645 - 541515\iota}) \\
 &\approx (-9 + \iota, -2174.219935 + 7969.975679\iota), \\
 P_2 &= (x_2, y_2) = (-4 - 3\iota, -20\sqrt{924613 - 1261876\iota}) \\
 &\approx (-4 - 3\iota, -22311.336861 + 11311.522997\iota), \\
 P_3 &= (x_3, y_3) = (1 + 2\iota, 10\sqrt{-1744002 + 734019\iota}) \\
 &\approx (1 + 2\iota, 2721.885087 + 13483.651524\iota), \\
 P_4 &= (x_4, y_4) = (6 + 4\iota, -4\sqrt{99702405 - 110095815\iota}) \\
 &\approx (6 + 4\iota, -44563.130818 + 19764.466810\iota).
 \end{aligned}
 \tag{37}$$

Actually, $y_i = y_+(x_i)$ for all i . Using the sequence of signs on Sheet a, and fig. 4, we

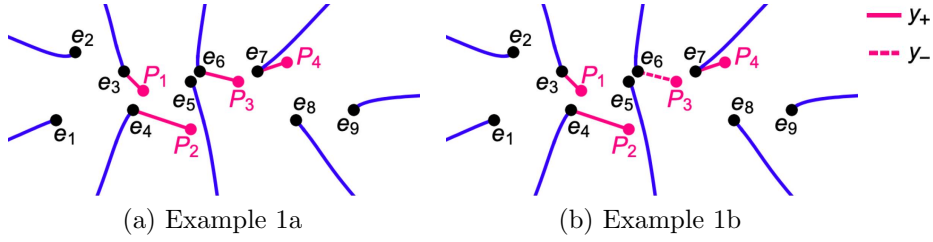


FIGURE 6. Paths to points of divisor D .

find that P_1, P_2, P_4 are located on Sheet a, and P_3 on Sheet b. Then we compute the corresponding Abel images, see locations of points P_i on fig. 6(a)

$$\begin{aligned}
 \mathcal{A}(P_1) &= \mathcal{A}_{0,1}^{[+]} + \sum_{i=1}^2 \mathcal{A}_{i,i+1}^{[-]} + \int_{e_3}^{x_1} du^{[+]}, \\
 \mathcal{A}(P_2) &= \mathcal{A}_{0,1}^{[+]} + \sum_{i=1}^3 \mathcal{A}_{i,i+1}^{[-]} + \int_{e_4}^{x_2} du^{[+]}, \\
 \mathcal{A}(P_3) &= -\left(\mathcal{A}_{0,1}^{[+]} + \sum_{i=1}^3 \mathcal{A}_{i,i+1}^{[-]} + \mathcal{A}_{4,5}^{[+]} + \mathcal{A}_{5,6}^{[-]} + \int_{e_6}^{x_3} du^{[-]} \right), \\
 \mathcal{A}(P_4) &= \mathcal{A}_{0,1}^{[+]} + \sum_{i=1}^3 \mathcal{A}_{i,i+1}^{[-]} + \mathcal{A}_{4,5}^{[+]} + \sum_{i=5}^6 \mathcal{A}_{i,i+1}^{[-]} + \int_{e_7}^{x_4} du^{[+]},
 \end{aligned}$$

and find

$$u(D) = \sum_{i=1}^4 \mathcal{A}(P_i) \approx \begin{pmatrix} -1.182750 + 0.205635\iota \\ 0.073714 - 0.038375\iota \\ -0.004762 + 0.002674\iota \\ 0.000592 - 0.000064\iota \end{pmatrix}.$$

By means of (12), with θ -function approximated by a partial sum of (6), $n_i \leq 5$, we obtain

$$(38) \quad \begin{aligned} \wp_{1,1}(u(D)) &\approx -6 + 4\iota, & \wp_{1,1,1}(u(D)) &\approx 91.581255 - 159.929002\iota, \\ \wp_{1,3}(u(D)) &\approx 42 + 53\iota, & \wp_{1,1,3}(u(D)) &\approx 23.849556 - 1665.831810\iota, \\ \wp_{1,5}(u(D)) &\approx 193 + 191\iota, & \wp_{1,1,5}(u(D)) &\approx -6971.970187 - 998.734510\iota, \\ \wp_{1,7}(u(D)) &\approx 446 - 578\iota, & \wp_{1,1,7}(u(D)) &\approx -5733.795768 - 18693.578334\iota. \end{aligned}$$

Next, we use the solution (15) of the Jacobi inversion problem to verify if the obtained Abel image corresponds to the given divisor D , and at the same time, to verify the compliance of the obtained periods with the curve. On a hyperelliptic curve of genus 4 this solution acquires the form

$$\mathcal{R}_8(x; u) \equiv x^4 - x^3\wp_{1,1}(u) - x^2\wp_{1,3}(u) - x\wp_{1,5}(u) - \wp_{1,7}(u) = 0,$$

$$\mathcal{R}_9(x, y; u) \equiv 2y + x^3\wp_{1,1,1}(u) + x^2\wp_{1,1,3}(u) + x\wp_{1,1,5}(u) + \wp_{1,1,7}(u) = 0.$$

The two polynomial functions \mathcal{R}_8 and \mathcal{R}_9 with coefficients (38) both vanish on the given D .

On the other hand, the common divisor of zeros of \mathcal{R}_8 and \mathcal{R}_9 , which is a degree g non-special divisor D_g , uniquely defines these two polynomial functions. With a divisor $D_4 = \sum_{i=1}^4 (x_i, y_i)$ on a genus 4 hyperelliptic curve, we have

$$\mathcal{R}_8(x; D_4) = \frac{\begin{vmatrix} x^4 & x^3 & x^2 & x & 1 \\ x_1^4 & x_1^3 & x_1^2 & x_1 & 1 \\ x_2^4 & x_2^3 & x_2^2 & x_2 & 1 \\ x_3^4 & x_3^3 & x_3^2 & x_3 & 1 \\ x_4^4 & x_4^3 & x_4^2 & x_4 & 1 \end{vmatrix}}{\begin{vmatrix} x_1^3 & x_1^2 & x_1 & 1 \\ x_2^3 & x_2^2 & x_2 & 1 \\ x_3^3 & x_3^2 & x_3 & 1 \\ x_4^3 & x_4^2 & x_4 & 1 \end{vmatrix}}, \quad \mathcal{R}_9(x, y; D_4) = 2 \frac{\begin{vmatrix} y & x^3 & x^2 & x & 1 \\ y_1 & x_1^3 & x_1^2 & x_1 & 1 \\ y_2 & x_2^3 & x_2^2 & x_2 & 1 \\ y_3 & x_3^3 & x_3^2 & x_3 & 1 \\ y_4 & x_4^3 & x_4^2 & x_4 & 1 \end{vmatrix}}{\begin{vmatrix} x_1^3 & x_1^2 & x_1 & 1 \\ x_2^3 & x_2^2 & x_2 & 1 \\ x_3^3 & x_3^2 & x_3 & 1 \\ x_4^3 & x_4^2 & x_4 & 1 \end{vmatrix}}.$$

Then, the given divisor D defined by (37) is the common divisor of zeros of the two polynomial functions

$$(39a) \quad \mathcal{R}_8(x; D) \equiv x^4 + (6 - 4\iota)x^3 - (42 + 53\iota)x^2 - (193 + 191\iota)x - 446 + 578\iota,$$

$$(39b) \quad \mathcal{R}_9(x, y; D) \equiv 2y + (91.581255 - 159.929002\iota)x^3 \\ + (23.849556 - 1665.831810\iota)x^2 - (6971.970187 + 998.734510\iota)x \\ - 5733.795768 - 18693.578334\iota.$$

Coefficients of \mathcal{R}_8 and \mathcal{R}_9 in (39) give values of \wp -functions at $u(D)$, which coincide with (38) with an accuracy of 10^{-12} .

4.2. Example 1b. Let D from Example 1a be slightly modified, by moving P_3 from Sheet b to Sheet a, where $y_3 = y_-(x_3)$. That is

$$P_3 = (x_3, y_3) = (1 + 2\iota, -10\sqrt{-1744002 + 734019\iota}) \\ \approx (1 + 2\iota, -2721.885087 - 13483.651524\iota).$$

Then $\mathcal{A}(P_3)$ is computed with the opposite sign:

$$\mathcal{A}(P_3) = \mathcal{A}_{0,1}^{[+]} + \sum_{i=1}^3 \mathcal{A}_{i,i+1}^{[-]} + \mathcal{A}_{4,5}^{[+]} + \mathcal{A}_{5,6}^{[-]} + \int_{e_6}^{x_3} du^{[-]}.$$

Thus,

$$u(D) = \sum_{i=1}^4 \mathcal{A}(P_i) \approx \begin{pmatrix} -1.574832 + 0.029543\iota \\ 0.073141 - 0.050092\iota \\ -0.003641 + 0.002439\iota \\ 0.000890 + 0.000121\iota \end{pmatrix}.$$

Values of $\wp_{1,2i-1}$, $i = 1, 2, 3, 4$, remain the same, within the accuracy. The new values of $\wp_{1,1,2i-1}$, are

$$(40) \quad \begin{aligned} \wp_{1,1,1}(u(D)) &\approx -51.390396 - 175.145987\iota, \\ \wp_{1,1,3}(u(D)) &\approx -1007.385975 - 1486.407403\iota, \\ \wp_{1,1,5}(u(D)) &\approx -3163.745380 + 5334.829741\iota, \\ \wp_{1,1,7}(u(D)) &\approx 10094.385116 + 25500.899104\iota. \end{aligned}$$

Evidently, \mathcal{R}_8 remains unchanged, since values of x_i are kept the same. The new function \mathcal{R}_9 acquires the form

$$\begin{aligned} \mathcal{R}_9(x, y) &= 2y - (51.390396 + 175.145987\iota)x^3 \\ &\quad - (1007.385975 + 1486.407403\iota)x^2 - (3163.745380 - 5334.829741\iota)x \\ &\quad \quad \quad + 10094.385116 + 25500.899104\iota, \end{aligned}$$

and its coefficients coincide with the values (40) with an accuracy of 10^{-10} .

5. PERIODS ON A TRIGONAL CURVE

5.1. Trigonal curves. A generic trigonal curve is defined by the equation

$$(41) \quad 0 = \tilde{f}(x, y) = -y^3 + y^2\mathcal{T}(x) + y\mathcal{Q}(x) + \mathcal{P}(x).$$

Let maximal degrees of polynomials \mathcal{P} , \mathcal{Q} , \mathcal{T} be as shown in the table below. The genus g of a curve is displayed in the last column.

$$\begin{array}{llll} \text{Case 1:} & \deg \mathcal{P} = 3\mathfrak{m} + 1, & \deg \mathcal{Q} = 2\mathfrak{m}, & \deg \mathcal{T} = \mathfrak{m}, & g = 3\mathfrak{m}; \\ \text{Case 2:} & \deg \mathcal{P} = 3\mathfrak{m} + 2, & \deg \mathcal{Q} = 2\mathfrak{m} + 1, & \deg \mathcal{T} = \mathfrak{m}, & g = 3\mathfrak{m} + 1; \\ \text{Case 3:} & \deg \mathcal{P} = 3\mathfrak{m} + 3, & \deg \mathcal{Q} = 2\mathfrak{m} + 2 & \deg \mathcal{T} = \mathfrak{m} + 1, & g = 3\mathfrak{m} + 1. \end{array}$$

Note, that $y^2\mathcal{T}(x)$ is eliminated by the map $y \mapsto \tilde{y} + \frac{1}{3}\mathcal{T}(x)$, which leads to

$$\begin{aligned} 0 &= \tilde{f}(x, \tilde{y}) = -\tilde{y}^3 + \tilde{\mathcal{Q}}(x)\tilde{y} + \tilde{\mathcal{P}}(x), \\ \tilde{\mathcal{Q}}(x) &= \mathcal{Q}(x) + \frac{1}{3}\mathcal{T}(x)^2, \\ \tilde{\mathcal{P}}(x) &= \mathcal{P}(x) + \frac{1}{3}\mathcal{Q}(x)\mathcal{T}(x) + \frac{2}{27}\mathcal{T}(x)^3. \end{aligned}$$

The discriminant of (41) is computed as follows

$$(42) \quad \Delta(x) = \tilde{\mathcal{P}}(x)^2 - \frac{4}{27}\tilde{\mathcal{Q}}(x)^3,$$

where

$$(43) \quad \deg \Delta = N = \begin{cases} 6\mathfrak{m} + 2, & \text{Case 1;} \\ 6\mathfrak{m} + 4, & \text{Case 2;} \\ 6\mathfrak{m} + 6, & \text{Case 3.} \end{cases}$$

The degree of Δ shows the number N of finite branch points $\{B_i = (e_i, h_i)\}_{i=1}^N$. In Case 3, a curve has $6\mathfrak{m} + 6$ branch points, all finite. In Cases 1 and 2, a curve has $N = 2(g + 1)$ finite branch points, and a double branch point at infinity. Let

ν_i be the ramification index of B_i . Each branch point is counted $\nu_i - 1$ times. We assume, that all finite branch points have the ramification index 2, and the branch point B_0 at infinity has $\nu_0 = 3$.

Cases 1 and 2 with $\mathcal{T}(x) \equiv 0$ represent (n, s) -curves, which serve as canonical forms of trigonal curves. In these cases, the genus is computed by the formula $g = \frac{1}{2}(n-1)(s-1)$, see [9]. Case 3 is obtained by a proper bi-rational transformation from Case 2, thus the both cases have the same Weierstrass gap sequence \mathfrak{W} . Therefore, classification of trigonal curves is based on Cases 1 and 2. The corresponding gap sequences are (each set is supposed to be ordered ascendingly)

$$\begin{aligned} \text{Case 1} \quad \mathfrak{W} &= \{3i-2 \mid i=1, \dots, \mathfrak{m}\} \cup \{3i-1 \mid i=1, \dots, 2\mathfrak{m}\}; \\ \text{Case 2} \quad \mathfrak{W} &= \{3i-1 \mid i=1, \dots, \mathfrak{m}\} \cup \{3i-2 \mid i=1, \dots, 2\mathfrak{m}+1\}. \end{aligned}$$

The Sato weight introduces an order relation in the space of monomials $y^j x^i$. These monomials are used to construct the equation of a curve, and differentials. The ordered lists of monomials in the both cases are

$$(44a) \quad \text{Case 1: } \mathfrak{M} = \{1, x, \dots, x^{\mathfrak{m}-1}, x^{\mathfrak{m}}, y, x^{\mathfrak{m}+1}, yx, \dots, x^{2\mathfrak{m}-1}, yx^{\mathfrak{m}-1}, x^{2\mathfrak{m}}, yx^{\mathfrak{m}}, y^2, x^{2\mathfrak{m}+1}, yx^{\mathfrak{m}+1}, \{y^2 x^i, x^{2\mathfrak{m}+1+i}, yx^{\mathfrak{m}+1+i} \mid i \in \mathbb{N}\}\},$$

$$(44b) \quad \text{Case 2: } \mathfrak{M} = \{1, x, \dots, x^{\mathfrak{m}-1}, x^{\mathfrak{m}}, y, x^{\mathfrak{m}+1}, yx, \dots, x^{2\mathfrak{m}-1}, yx^{\mathfrak{m}-1}, x^{2\mathfrak{m}}, yx^{\mathfrak{m}}, x^{2\mathfrak{m}+1}, y^2, yx^{\mathfrak{m}+1}, x^{2\mathfrak{m}+2}, \{y^2 x^i, yx^{\mathfrak{m}+1+i}, x^{2\mathfrak{m}+2+i} \mid i \in \mathbb{N}\}\}.$$

5.2. Riemann surface. In what follows, we focus on the canonical forms of trigonal curves

$$(45) \quad 0 = f(x, y) = -y^3 + y\mathcal{Q}(x) + \mathcal{P}(x).$$

with the discriminant polynomial

$$\Delta(x) = \mathcal{P}(x)^2 - \frac{4}{27}\mathcal{Q}(x)^3.$$

Suppose, that all roots of Δ are distinct, also \mathcal{P} and \mathcal{Q} have no common roots. These conditions are sufficient for having only branch points with the ramification index 2.

Solutions of (45) are given by Cardano's formula:

$$(46a) \quad \begin{aligned} y_{+,a}(x) &= q_{+,a}(x) + \frac{1}{3}\mathcal{Q}(x)q_{+,a}^{-1}(x), \quad a = 1, 2, 3, \\ q_{+,a}(x) &= v_+^{1/3}(x)e^{2(a-1)\iota\pi/3}, \quad v_+(x) = \frac{1}{2}\left(\mathcal{P}(x) + \sqrt{\Delta(x)}\right), \end{aligned}$$

or equivalently

$$(46b) \quad \begin{aligned} y_{-,a}(x) &= q_{-,a}(x) + \frac{1}{3}\mathcal{Q}(x)q_{-,a}^{-1}(x), \quad a = 1, 2, 3, \\ q_{-,a}(x) &= v_-^{1/3}(x)e^{2(a-1)\iota\pi/3}, \quad v_-(x) = \frac{1}{2}\left(\mathcal{P}(x) - \sqrt{\Delta(x)}\right), \end{aligned}$$

where $\sqrt{\Delta}$ is defined by (23). By $q_{s,a}$, $s = \pm 1$, $a = 1, 2, 3$, three cubic roots of v_s are denoted. Let

$$(47) \quad v_s^{1/3}(x) = \begin{cases} |v_s(x)|^{1/3} e^{(\iota/3) \arg v_s(x)} & \text{if } \arg v_s(x) \geq 0, \\ |v_s(x)|^{1/3} e^{(\iota/3) \arg v_s(x) + \iota 2\pi/3} & \text{if } \arg v_s(x) < 0. \end{cases}$$

According to this definition, the function $v_s^{1/3}$ has the range $[0, \frac{2}{3}\pi)$, and its discontinuity is located over the contour $\Upsilon_s = \{x \mid \arg v_s(x) = 0\}$.

Theorem 2. *Let $v_s^{1/3}$ be defined by (47). Then each $y_{s,a}$ defined by (46) has discontinuity over the contour $\Upsilon_s = \{x \mid \arg v_s(x) = 0\}$. Along a path from a region with $\arg v_s(x) < 0$ to a region with $\arg v_s(x) \geq 0$ the analytic continuation of $y_{s,a}$ is given by $y_{s,b}$, where $a \mapsto b$ according to one of cyclic permutations (123) or (132).*

Proof. Let $s = +1$, and \tilde{x} be located in the vicinity of the contour Υ_+ , more precisely $|\arg v_+(\tilde{x})| < 3\phi$, with a small positive value ϕ . Then $0 \leq \arg v_+^{1/3}(\tilde{x}) < \phi$ if $\arg v_+(\tilde{x}) \geq 0$, and $\frac{2}{3}\pi - \phi < \arg v_+^{1/3}(\tilde{x}) < \frac{2}{3}\pi$ if $v_+(\tilde{x}) < 0$. Therefore, Υ_+ is the contour of discontinuity of $v_+^{1/3}$.

Now, we find how the three values $q_{+,a}$ of $v_+^{1/3}$ are connected over Υ_+ . Let $U(x_0; \delta)$ be a disc of radius δ with the center at $x_0 \in \Upsilon_+$. The contour Υ_+ divides the disc into two parts: U_+ where $\arg v_+(x) \geq 0$, and U_- where $\arg v_+(x) < 0$. Let $3\phi_+ = \max_{\tilde{x} \in U_+} \arg v_+(\tilde{x})$, then the range of $\arg v_+^{1/3}$ on U_+ is $[0, \phi_+)$. Let $-3\phi_- = \min_{\tilde{x} \in U_-} \arg v_+(\tilde{x})$, then the range of $\arg v_+^{1/3}$ on U_- is $(\frac{2}{3}\pi - \phi_-, \frac{2}{3}\pi)$. The analytic continuation of $v_+^{1/3}(x) = q_{+,1}(x)$ from U_+ to U_- is given by $e^{-\frac{2}{3}i\pi} v_+^{1/3}(x) = q_{+,3}(x)$, since the range of $\arg q_{+,3}$ on U_- is $(-\phi_-, 0)$, and so continuously connects to $q_{+,1}$ with the range $[0, \phi_+)$ on U_+ . Similarly, the analytic continuation of $v_+^{1/3}(x) = q_{+,1}(x)$ from U_- to U_+ is given by $e^{\frac{2}{3}i\pi} v_+^{1/3}(x) = q_{+,2}(x)$. Therefore, along a path from U_- to U_+ , the function $q_{+,1}$ continuously connects to $q_{+,2}$, then $q_{+,2}$ connects to $q_{+,3}$, and $q_{+,3}$ connects to $q_{+,1}$.

The same is true for $s = -1$. □

Theorem 3. *Let $\sqrt{\Delta}$ be defined by (23). Then among three values of y , given by (46a), or (46b), two have discontinuity over the contour $\Gamma = \{x \mid \arg \Delta(x) = 0\}$. If Γ_i is a segment of Γ which starts at a branch point $B_i = (e_i, h_i)$, where $h_i = y_a(e_i) = y_b(e_i)$, then y_a, y_b are discontinuous over Γ_i , and y_a serves as the analytic continuation of y_b on the other side of Γ_i , and vice versa.*

Proof. According to Theorem 1, the both functions v_+, v_- , defined in (46), have discontinuity over the contour $\Gamma = \{x \mid \arg \Delta(x) = 0\}$, and serve as analytic continuations of each other. This implies that all $q_{s,a}$ have discontinuity over Γ , and for every a the analytic continuation of $q_{+,a}$ is given by $q_{-,a}$, and vice versa. We assume that $y_{+,a}$, $a = 1, 2, 3$, have discontinuity over Γ , which follows from the same property of $q_{+,a}$.

Recall the relation $v_+^{1/3}(x)v_-^{1/3}(x) = \frac{1}{3}e^{2n\pi/3}Q(x)$, where $n = 0, 1$, or 2 such that $\arg v_+(x) + \arg v_-(x) = 3\arg Q(x) + 2\pi n$ holds in the vicinity of x . This implies three equalities of the form $y_{+,a_1}(x) = y_{-,a_2}(x)$, where $a_1 \mapsto a_2$ according to one of the transpositions: (12), (13), or (23). Indeed,

$$\begin{aligned} n = 0 & \quad y_{+,1}(x) = y_{-,1}(x), \quad y_{+,2}(x) = y_{-,3}(x), \quad y_{+,3}(x) = y_{-,2}(x); \\ n = 1 & \quad y_{+,1}(x) = y_{-,3}(x), \quad y_{+,2}(x) = y_{-,2}(x), \quad y_{+,3}(x) = y_{-,1}(x); \\ n = 2 & \quad y_{+,1}(x) = y_{-,2}(x), \quad y_{+,2}(x) = y_{-,1}(x), \quad y_{+,3}(x) = y_{-,3}(x). \end{aligned}$$

Taking into account, that over Γ at every a the analytic continuation of $y_{+,a}$ is given by $y_{-,a}$, we see that among the three values of y given by (46a), or (46b), one remains continuous, and the other two serve as analytic continuations of each other. Indeed, let $n = 0$ in the vicinity of x , then $y_{+,1}(x) = y_{-,1}(x)$. If a segment of Γ is located in the vicinity of x , then $y_{-,1}$ serves as the analytic continuation of $y_{+,1}$ on the other side of the segment, and so $y_{+,1}$ remains continuous. At the same

time, $y_{-,2}(x) = y_{+,3}(x)$ serves as the analytic continuation of $y_{+,2}(x) = y_{-,3}(x)$, as follows from Theorem 1.

The contour Γ consists of segments Γ_i , each starts at e_i such that $B_i = (e_i, h_i)$ is a branch point, and ends at infinity. Let $x_0 \in \Gamma_i$ be located in the vicinity of e_i which does not contain Υ_+ , and $h_i = y_{+,a}(e_i) = y_{+,b}(e_i)$. Let $U(x_0, \delta)$ be a disc of radius δ centered at x_0 , such that $|x_0 - e_i| \geq \delta$. Then $U(x_0, \delta)$ is divided by Γ_i into two parts: U_+ where $\arg \Delta(x) \geq 0$, and U_- where $\arg \Delta(x) < 0$. There exists such c that $y_{+,c}(x) = y_{-,c}(x)$ for every $x \in U(x_0, \delta)$, and so $y_{+,c}$ is continuous over $U(x_0, \delta)$. Then a, b are the other two values from $\{1, 2, 3\}$, since $y_{+,a}(x) = y_{-,b}(x)$ and $y_{+,b}(x) = y_{-,a}(x)$ over $U(x_0, \delta)$. Indeed, due to $\Delta(e_i) = 0$ we have $y_{+,a}(e_i) = y_{+,b}(e_i)$.

Similar considerations can be made in the case of $\mathbf{s} = -1$. \square

In what follows, we work with solutions $y_{+,a}$, $a = 1, 2, 3$, computed by the formula (46a), and denote them by y_a .

5.3. Monodromy path. In order to construct a model of the Riemann surface, a monodromy path γ , which is a continuous path through all branch points, should be chosen. Based on the investigation presented in subsection 5.2, the following algorithm is suggested.

1. Find all finite branch points $\{B_i = (e_i, h_i)\}_{i=1}^N$, and sort ascendingly first by $\operatorname{Re} e_i$, then by $\operatorname{Im} e_i$. The points are enumerated according to this order. Each point B_i is labeled by 'a-b', such that $h_i = y_a(e_i) = y_b(e_i)$, which means that solutions y_a and y_b connect over the segment Γ_i , which goes from e_i to infinity.
2. According to this order, a continuous path γ on the Riemann sphere through all e_i is constructed from straight line segments $[e_i, e_{i+1}]$, $i = 1, \dots, N$. Then the segment $(-\infty, e_1]$ is added at the beginning of the polygonal path γ , and $[e_N, \infty)$ at the end.
3. Plot the contour $\Gamma = \{x \mid \arg \Delta(x) = 0\}$, see blue contours on fig. 7, and the contour $\Upsilon_+ = \{x \mid \arg v_+(x) = 0\}$, see green contours on fig. 7. Identify a permutation which corresponds to each segment of Γ_i , and Υ_+ . When the path γ crosses Γ_i , solutions y_a and y_b interchange. When γ crosses Υ_+ , solutions y_a, y_b, y_c permute in the corresponding cycle.
4. Moving along the monodromy path γ from the left to the right, passing e_i and cuts from the below, counter-clockwise, and taking into account intersections with Γ and Υ_+ , find the sequence of changes of solutions y_a , $a = 1, 2, 3$, starting from 1, 2, and 3, respectively:

$$\begin{aligned} \text{Sheet a:} & \quad \{\mathbf{a}_{0,1} = 1\} \cup \{\mathbf{a}_{i,i+1}\}_{i=1}^{N-1} \cup \{\mathbf{a}_{N,0}\}, \\ \text{Sheet b:} & \quad \{\mathbf{b}_{0,1} = 2\} \cup \{\mathbf{b}_{i,i+1}\}_{i=1}^{N-1} \cup \{\mathbf{b}_{N,0}\}, \\ \text{Sheet c:} & \quad \{\mathbf{c}_{0,1} = 3\} \cup \{\mathbf{c}_{i,i+1}\}_{i=1}^{N-1} \cup \{\mathbf{c}_{N,0}\}. \end{aligned}$$

Index 0 stands for infinity. Each sequence marks a sheet of the Riemann surface.

The monodromy path γ lifted to each sheet, and closed by a semi-circle around infinity in the counter-clockwise direction, is homotopic to zero.

5.4. Homology. Note, that $N = 2(g+1)$ on a canonical trigonal curve. Therefore, finite branch points split into $g+1$ pairs. Without loss of generality, g cuts are made between branch points in pairs B_{2i}, B_{2i+1} , $i = 1, \dots, g$. Each cut goes through

finite points, on the two sheets connected by branch points in a pair. One more cut is made from B_1 to B_N through infinity.

Let \mathbf{a}_i encircle the cut (B_{2i}, B_{2i+1}) counter-clockwise. Let \mathbf{b}_i emerge from the cut $(B_1, \infty) \cup (\infty, B_N)$, and enter the cut encircled by \mathbf{a}_i . In this way a canonical homology basis is obtained.

5.5. Cohomology. First kind differentials are constructed with the help of the first g monomials from the ordered list \mathfrak{M} , namely:

$$(48) \quad du_{\mathbf{w}_i} = \frac{\mathbf{m}_{g-i+1}(x, y) dx}{\partial_y f(x, y)}, \quad i = 1, \dots, g,$$

where \mathbf{m}_k is the k -th element of \mathfrak{M} , and \mathbf{w}_i are elements of the gap sequence \mathfrak{W} .

A second kind differential $dr_{\mathbf{w}_i}$ is constructed with the help of the first $g+i$ monomials from \mathfrak{M} . Namely

$$(49) \quad dr_{\mathbf{w}_i} = \left(\sum_{j=1}^{g+i} c_{i,j} \mathbf{m}_j(x, y) \right) \frac{dx}{\partial_y f(x, y)}, \quad i = 1, \dots, g.$$

The relation (10) defines the coefficients of monomials \mathbf{m}_{g+i} , $i \geq 1$. Coefficients of the remaining part of the sum in (49) are also essential. In the case of trigonal curves, the second kind differentials associated to the standard first kind differentials (48) are obtained in [11], by means of the Klein formula.

5.6. Computation of periods. Next, first kind integrals on each segment along the polygonal monodromy path γ are computed:

$$(50a) \quad \mathcal{A}_{i,i+1}^{[n_{i,i+1}]} = \int_{e_i}^{e_{i+1}} du^{[n_{i,i+1}]}, \quad i = 1, \dots, N-1,$$

$$(50b) \quad \mathcal{A}_{0,1}^{[n_{0,1}]} = \int_{-\infty}^{e_1} du^{[n_{0,1}]}, \quad \mathcal{A}_{N,0}^{[n_{N,0}]} = \int_{e_N}^{\infty} du^{[n_{N,0}]},$$

where $\mathbf{n} = \mathbf{a}, \mathbf{b}$, or \mathbf{c} , depending on the sheet. The integrand of $\mathcal{A}_{i,j}^{[n_{i,j}]}$ is defined by (48) with $y = y_{n_{i,j}}(x)$. A lift of the monodromy path γ to each sheet, closed by a semi-circle around infinity in the counter-clockwise direction, is homotopic to zero, and so relations hold

$$(51) \quad \mathcal{A}_{0,1}^{[n_{0,1}]} + \sum_{i=1}^{N-1} \mathcal{A}_{i,i+1}^{[n_{i,i+1}]} + \mathcal{A}_{N,0}^{[n_{N,0}]} = 0, \quad \mathbf{n} = \mathbf{a}, \mathbf{b}, \mathbf{c},$$

which serve for verification.

With a chosen basis of canonical cycles, first kind period matrices ω , and ω' are computed by (4), and the normalized period matrix is obtained by

$$\tau = \omega^{-1} \omega'.$$

The latter is required to be symmetric with a positive imaginary part.

With the same basis of canonical cycles, second kind period matrices η , and η' are computed by (9) with differentials (49). Then the symmetric matrix \varkappa from the definition of σ -function is obtained by

$$\varkappa = \eta \omega^{-1}.$$

First and second kind period matrices satisfy the Legendre relation (11).

5.7. Example 3: (3,4)-curve. We consider the simplest trigonal curve in its canonical form

$$(52) \quad 0 = f(x, y) = -y^3 + x^4 + \lambda_2 y x^2 + \lambda_3 x^3 + \lambda_5 y x + \lambda_6 x^2 + \lambda_8 y + \lambda_9 x + \lambda_{12}.$$

From $\Delta(x) = 0$ we find x -coordinates e_i of branch points $B_i = (e_i, h_i)$. Then using (46a), we find the corresponding values $y_a(e_i)$, $a = 1, 2, 3$, two of which, say a and b , coincide and give h_i . So each branch point is labeled by ‘ a - b ’, that indicates which solutions connect in the vicinity of B_i .

A (3,4)-curve possesses the gap sequence $\mathfrak{W} = \{1, 2, 5\}$, and the first kind differentials have the form

$$du = \begin{pmatrix} du_1 \\ du_2 \\ du_5 \end{pmatrix} = \begin{pmatrix} y \\ x \\ 1 \end{pmatrix} \frac{dx}{-3y^2 + \mathcal{Q}(x)}.$$

Let $\mathcal{A}_{i,j}^{[a]}$ denote a first kind integral between e_i and e_j computed with $y = y_a(x)$:

$$(53) \quad \mathcal{A}_{i,j}^{[a]} = \int_{e_i}^{e_j} du^{[a]}.$$

Second kind differentials associated with the first ones on the curve (52) are defined as follows

$$dr = \begin{pmatrix} dr_1 \\ dr_2 \\ dr_5 \end{pmatrix} = \begin{pmatrix} x^2 \\ 2xy \\ R_5 \end{pmatrix} \frac{dx}{-3y^2 + \mathcal{Q}(x)},$$

$$R_5 = 5x^2y + 3\lambda_3xy + \frac{2}{3}\lambda_2^2x^2 + \lambda_6y + \frac{2}{3}\lambda_2\lambda_5x.$$

A second kind integral $\mathcal{B}_{i,j}^{[a]}$ between e_i and e_j with $y = y_a(x)$ is computed by

$$(54) \quad \mathcal{B}_{i,j}^{[a]} = \int_{B_i}^{B_j} dr^{[a]}.$$

As an example, we consider a curve defined by the equation

$$(55) \quad 0 = f(x, y) \equiv -y^3 + x^4 + y(4x^2 + 5x + 11) + 3x^3 + 7x^2 + 16x + 9.$$

The curve has eight finite branch points:

$e_1 \approx -4.58931,$	$h_1 \approx -4.9092$	2-3
$e_2 \approx -1.17922 - 0.934455\iota,$	$h_2 \approx 1.60505 + 0.430221\iota$	1-3
$e_3 \approx -1.17922 + 0.934455\iota,$	$h_3 \approx 1.60505 - 0.430221\iota$	1-3
$e_4 \approx -0.431732 - 2.20256\iota,$	$h_4 \approx 0.309255 - 1.83532\iota$	2-3
$e_5 \approx -0.431732 + 2.20256\iota,$	$h_5 \approx 0.309255 + 1.83532\iota$	1-2
$e_6 \approx 0.499118 - 1.57527\iota,$	$h_6 \approx -1.80047 + 1.31135\iota$	1-2
$e_7 \approx 0.499118 + 1.57527\iota,$	$h_7 \approx -1.80047 - 1.31135\iota$	2-3
$e_8 \approx 0.812986,$	$h_8 \approx -2.42959$	2-3

In the last column the corresponding pairs ‘ a - b ’ are indicated.

Fig. 7(a) displays positions of e_i , and the contours where solutions y_a , $a = 1, 2, 3$, have discontinuity. The contour $\Upsilon_+ = \{x \mid \arg v_+(x) = 0\}$ is marked in green. Over Υ_+ all three solutions connect in pairs. Each segment of Υ_+ is labeled by the cyclic permutation (123), and an arrow shows in which direction this permutation occurs.

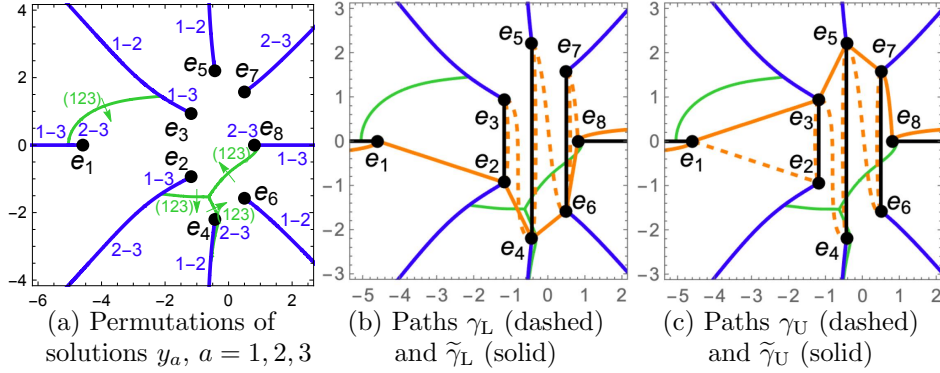


FIGURE 7. Contours Γ (blue), Υ_+ (green), cuts (black), and a path (orange).

The contour $\Gamma = \{x \mid \arg \Delta(x) = 0\}$ is marked in blue. Each segment Γ_i of Γ starts at e_i and ends at infinity. Let $h_i = y_a(e_i) = y_b(e_i)$, then Γ_i is labeled by ‘ a - b ’ in the vicinity of e_i . If Υ_+ intersects Γ_i at a point d_i , then the segment of Γ_i between d_i and infinity is labeled by ‘ b - c ’ such that $y_b(x) = y_c(x)$ for all x on this segment. Fig. 7(a) is in accordance with the density plots of $\arg y_a$, $a = 1, 2, 3$, shown on fig. 8.

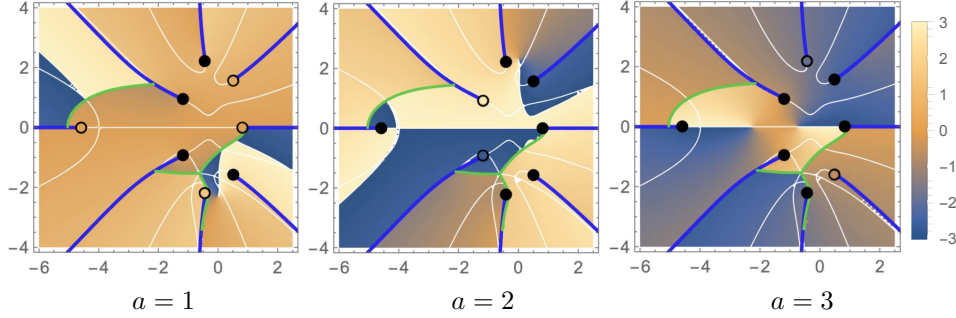


FIGURE 8. Density plot of $\arg y_a$, contours Γ (blue), Υ_+ (green).

Cuts connect pairs of points: B_2 and B_3 on sheets with solutions y_1 and y_3 ; B_4 and B_5 on sheets with solutions y_1 and y_2 in the vicinity of B_5 which change consequently into the pair 1-3 and then 2-3 when approaching B_4 ; B_6 and B_7 on sheets with solutions y_2 and y_3 in the vicinity of B_7 which change into the pair 1-2 when approaching B_6 . One more cut goes from B_8 to infinity, and then to B_1 . In the vicinity of B_8 solutions y_2 and y_3 connect, which change into the pair 1-3 in the vicinity of infinity, and then into 2-3 in the vicinity of B_1 .

Let the monodromy path γ_L through all branch points be

$$\begin{aligned} &(-\infty, e_1] \cup [e_1, e_2] \cup [e_2, e_3] \cup [e_3, e_4] \cup [e_4, e_5] \\ &\cup [e_5, e_6] \cup [e_6, e_7] \cup [e_7, e_8] \cup [e_8, \infty), \end{aligned}$$

as shown on fig. 7(b) in orange. The path is polygonal, and goes below points e_i and cuts, and so rounds cuts and branch points counter-clockwise. The path γ_L

is marked by dashed lines between e_2 and e_8 , and continuously deformed into a simpler path $\tilde{\gamma}_L$, which is marked by solid lines, and goes below points e_2, e_4, e_6 .

Sheets are marked according to the monodromy path γ_L , namely

$$(56) \quad \begin{aligned} & \{a_{0,1}, a_{1,2}, a_{2,3}, a_{3,4}, a_{4,5}, a_{5,6}, a_{6,7}, a_{7,8}, a_{8,0}\} = \\ \text{Sheet a: } & \{ 1, 1, 3, 3-1, 1-2-3, 3-2, 1-2, 2, 3 \}, \\ & \{b_{0,1}, b_{1,2}, b_{2,3}, b_{3,4}, b_{4,5}, b_{5,6}, b_{6,7}, b_{7,8}, b_{8,0}\} = \\ \text{Sheet b: } & \{ 2, 2, 2, 2-3, 2-3-1, 1-3, 3-1, 1, 1 \}, \\ & \{c_{0,1}, c_{1,2}, c_{2,3}, c_{3,4}, c_{4,5}, c_{5,6}, c_{6,7}, c_{7,8}, c_{8,0}\} = \\ \text{Sheet c: } & \{ 3, 3, 1, 1-2, 3-1-2, 2-1, 2-3, 3, 2 \}. \end{aligned}$$

Connection of solutions y_1, y_2, y_3 on each sheet is shown on fig. 9.

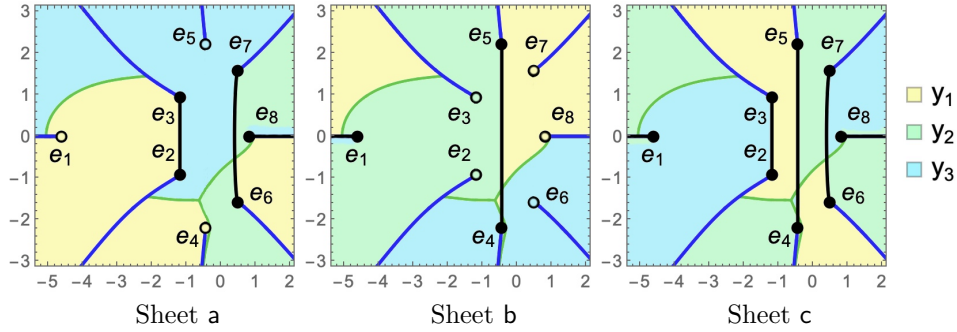


FIGURE 9. Connection of solutions y_1, y_2, y_3 on each sheet.

On fig. 7(c) an alternative monodromy path γ_U is presented, marked by dashed lines between e_1 and e_7 . The path γ_U goes from the right to the left above points e_i and cuts, which are rounded counter-clockwise. γ_U is continuously deformed into a simpler path $\tilde{\gamma}_U$, which is marked by solid lines, and goes above points e_3, e_5, e_7 .

One can see that the cuts (B_2, B_3) , and (B_6, B_7) connect Sheets a and c, and the cut (B_4, B_5) connects Sheets b and c. The cut $(B_8, \infty) \cup (\infty, B_1)$ connects Sheets a and c on segment $[e_8, \infty)$, and Sheets b and c on $(\infty, e_1]$.

Moving along the path $\tilde{\gamma}_L$ from the left to the right, rounding infinity clockwise, and then moving along the path $\tilde{\gamma}_U$ from the right to the left, a circle γ_∞ around infinity on the Riemann sphere is drawn. Then γ_∞ is lifted to the curve.

Let the lift of γ_∞ start at B_1 on Sheet c, and reach B_8 along $\tilde{\gamma}_L^c$, the lift of $\tilde{\gamma}_L$ to Sheet c. The analytic continuation of y_3 on Sheet c is y_2 on Sheet a on the other side of Γ_8 in the vicinity of e_8 . So the path enters the cut and emerges on Sheet a, where segment $[e_8, \infty + i\epsilon)$ is governed by y_2 . The path continues on Sheet a along $\tilde{\gamma}_U^a$, the lift of $\tilde{\gamma}_U$ to Sheet a, and reaches the point $(e_1, y_1(e_1))$, which is not a branch point. Thus, one full turn around infinity, denoted by $\tilde{\gamma}_\infty^{c-a}$, is completed. The path continues on Sheet a along $\tilde{\gamma}_L^a$, and reaches B_8 . Solution y_2 on Sheet a connects to y_3 on Sheet c on the other side of Γ_8 in the vicinity of e_8 . So, the path moves from Sheet a to Sheet c, where segment $[e_8, \infty + i\epsilon)$ is governed by y_3 . Then the path goes on Sheet c along $\tilde{\gamma}_U^c$, and reaches B_1 . At this point the second turn around infinity, denoted by $\tilde{\gamma}_\infty^{a-c}$, is completed. In the vicinity of e_1 solution y_3 on Sheet c connects to y_2 on Sheet b. So the path enters the cut and emerges on Sheet b, then goes on Sheet b along $\tilde{\gamma}_L^b$, and reaches the point $(e_8, y_1(e_8))$, then continues on Sheet b along $\tilde{\gamma}_U^b$, and reaches B_1 . The third turn around infinity, denoted by $\tilde{\gamma}_\infty^{b-b}$, is completed by

the arrival to the initial point. The lift of γ_∞ , which is $\tilde{\gamma}_{3\infty} \equiv \tilde{\gamma}_\infty^{c-a} \cup \tilde{\gamma}_\infty^{a-c} \cup \tilde{\gamma}_\infty^{b-b}$, can be used to reach an arbitrary point on the curve.

In fact, $\mathfrak{a}_{8,0}$, $\mathfrak{c}_{8,0}$ in the sequences (56) do not belong to the sheets where they are listed. But the indicated paths, closed by a semi-circle around infinity in the counter-clockwise direction, are homotopic to zero. Correspondingly, the sum of first kind integrals along each path vanishes. Then the following relations are obtained along the simpler path $\tilde{\gamma}_L$:

$$(57) \quad \begin{aligned} \mathcal{A}_{0-,1}^{[1]} + \mathcal{A}_{1,2}^{[1]} + \mathcal{A}_{2,4}^{[3-1]} + \mathcal{A}_{4,6}^{[1-2]} + \mathcal{A}_{6,8}^{[1-2]} + \mathcal{A}_{8,0+}^{[3]} &= 0, \\ \mathcal{A}_{0-,1}^{[2]} + \mathcal{A}_{1,2}^{[2]} + \mathcal{A}_{2,4}^{[2-3]} + \mathcal{A}_{4,6}^{[2-3]} + \mathcal{A}_{6,8}^{[3-1]} + \mathcal{A}_{8,0+}^{[1]} &= 0, \\ \mathcal{A}_{0-,1}^{[3]} + \mathcal{A}_{1,2}^{[3]} + \mathcal{A}_{2,4}^{[1-2]} + \mathcal{A}_{4,6}^{[3-1]} + \mathcal{A}_{6,8}^{[2-3]} + \mathcal{A}_{8,0+}^{[2]} &= 0. \end{aligned}$$

Here $0-$ ($0+$) stands for $-\infty - \iota\epsilon$ ($\infty + \iota\epsilon$), and the superscript of $\mathcal{A}_{i,j}^{[a-b]}$ indicates that over the segment $[e_i, e_j]$ solution y_a changes into y_b . Note, the last relation follows from the first two, due to $\mathcal{A}_{i,j}^{[a_i,j]} + \mathcal{A}_{i,j}^{[b_i,j]} + \mathcal{A}_{i,j}^{[c_i,j]} = 0$, where $\mathfrak{a}_{i,j}$, $\mathfrak{b}_{i,j}$, and $\mathfrak{c}_{i,j}$ correspond to Sheets \mathfrak{a} , \mathfrak{b} , and \mathfrak{c} .

Let the path $\tilde{\gamma}_U$, starting at $\infty + \iota\epsilon$ and ending at $-\infty - \iota\epsilon$, be closed by a semi-circle around infinity in the counter-clockwise direction. On each sheet this path is homotopic to zero, and so produces another set of relations:

$$(58) \quad \begin{aligned} \mathcal{A}_{0+,8}^{[3]} + \mathcal{A}_{8,7}^{[2]} + \mathcal{A}_{7,5}^{[3]} + \mathcal{A}_{5,3}^{[3]} + \mathcal{A}_{3,1}^{[1]} + \mathcal{A}_{1,0-}^{[1]} &= 0, \\ \mathcal{A}_{0+,8}^{[2]} + \mathcal{A}_{8,7}^{[3]} + \mathcal{A}_{7,5}^{[2]} + \mathcal{A}_{5,3}^{[1]} + \mathcal{A}_{1,3}^{[3]} + \mathcal{A}_{1,0-}^{[2]} &= 0, \\ \mathcal{A}_{0+,8}^{[1]} + \mathcal{A}_{8,7}^{[1]} + \mathcal{A}_{7,5}^{[1]} + \mathcal{A}_{5,3}^{[2]} + \mathcal{A}_{3,1}^{[2]} + \mathcal{A}_{1,0-}^{[3]} &= 0. \end{aligned}$$

Note, that all branch points can be reached on Sheet \mathfrak{c} , as well as all cuts. Let \mathfrak{a} -cycles be located on Sheet \mathfrak{c} , encircling the three finite cuts. Let \mathfrak{b}_i -cycle emerge from the cut $(B_8, \infty) \cup (\infty, B_1)$, and enter the cut encircled by \mathfrak{a}_i -cycle, see fig. 10. Therefore, \mathfrak{b}_1 and \mathfrak{b}_3 go through Sheets \mathfrak{c} and \mathfrak{a} , then \mathfrak{b}_2 goes through Sheets \mathfrak{c} and \mathfrak{b} . Periods are calculated according to fig. 10, as follows

$$\begin{aligned} \omega_1 &= \mathcal{A}_{2,3}^{[1]} + \mathcal{A}_{3,2}^{[3]}, \\ \omega_2 &= \mathcal{A}_{4,5}^{[3-1-2]} + \mathcal{A}_{5,4}^{[1-3-2]} = \mathcal{A}_{4,6}^{[3-1]} + \mathcal{A}_{6,5}^{[1-2]} + \mathcal{A}_{5,2}^{[1]} + \mathcal{A}_{2,4}^{[1-2]}, \\ \omega_3 &= \mathcal{A}_{6,7}^{[2-3]} + \mathcal{A}_{7,6}^{[2-1]}, \\ \omega'_1 &= \mathcal{A}_{8,7}^{[3]} + \mathcal{A}_{7,5}^{[2]} + \mathcal{A}_{5,3}^{[1]} + \mathcal{A}_{3,6}^{[3-2]} + \mathcal{A}_{6,8}^{[1-2]}, \\ \omega'_2 &= \mathcal{A}_{1,2}^{[3]} + \mathcal{A}_{2,4}^{[1-2]} + \mathcal{A}_{4,2}^{[3-2]} + \mathcal{A}_{2,1}^{[2]}, \\ \omega'_3 &= \mathcal{A}_{8,7}^{[3]} + \mathcal{A}_{7,8}^{[2]}. \end{aligned}$$

Computation of $\mathcal{A}_{i,j}^{[n_i,j]}$ is performed with the help of `NIntegrate` with a working precision of 18. The relations (57) and (58) are satisfied with an accuracy of 10^{-15} .

The following not normalized period matrices are obtained

$$\omega \approx \begin{pmatrix} -0.646716\iota & 1.367235\iota & -1.406214\iota \\ 0.557691\iota & 0.662524\iota & 0.237700\iota \\ -0.425220\iota & -0.085658\iota & 0.761823\iota \end{pmatrix},$$

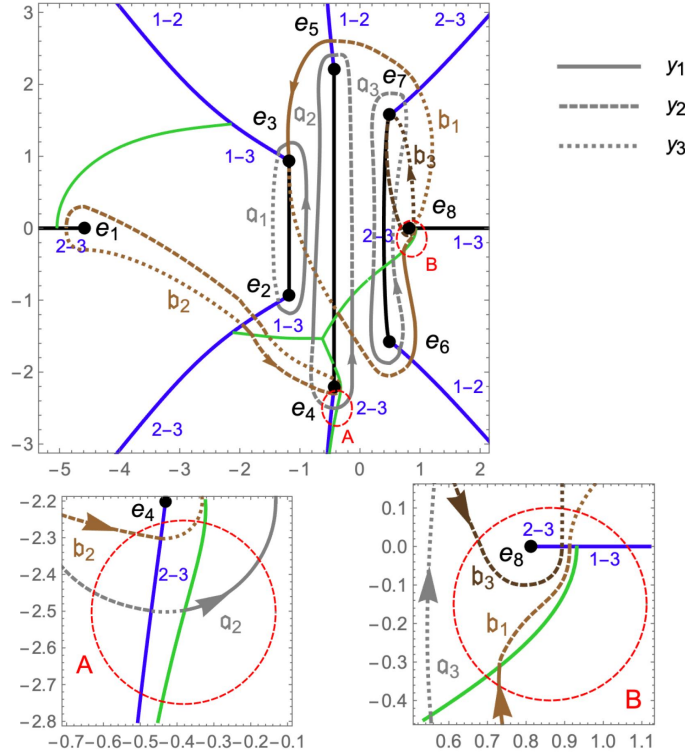


FIGURE 10. Canonical homology basis.

$$\omega' \approx \begin{pmatrix} 1.114221 + 0.360259i & -0.838244 + 0.360259i & 0.830310 - 0.703107i \\ -0.888801 + 0.610108i & -0.725076 + 0.610108i & -0.483530 + 0.118850i \\ 0.212490 - 0.255439i & 0.017209 - 0.255439i & -0.244951 + 0.380911i \end{pmatrix},$$

and the normalized period matrix from the Siegel upper half-space

$$\tau \approx \begin{pmatrix} 0.5 + 1.204054i & 0.5 + 0.179707i & 0.413339i \\ 0.5 + 0.179707i & 0.5 + 0.879769i & 0.176635i \\ 0.413339i & 0.176635i & 0.5 + 0.572103i \end{pmatrix}.$$

Second kind period matrices are

$$\eta \approx \begin{pmatrix} -0.541959i & -0.385425i & -0.722057i \\ 1.52536i & -0.88414i & 0.484784i \\ 0.975636i & -1.01088i & -2.65892i \end{pmatrix},$$

$$\eta' \approx \begin{pmatrix} -1.357307 - 0.463692i & 2.945439 - 0.463692i & -0.354124 - 0.361028i \\ 2.292766 + 0.320609i & 5.356432 + 0.320609i & 2.131611 + 0.242392i \\ -5.584050 - 0.017623i & 4.038588 - 0.017623i & 6.689080 - 1.329459i \end{pmatrix},$$

and the symmetric matrix \varkappa is

$$\varkappa \approx \begin{pmatrix} 0.180731 & -0.994032 & -0.304044 \\ -0.994032 & 0.540116 & -1.367017 \\ -0.304044 & -1.367017 & -3.624898 \end{pmatrix}.$$

The symmetric property of τ is satisfied with an accuracy of 10^{-15} , and of \varkappa with an accuracy of 10^{-13} .

6. COMPUTATION OF \wp -FUNCTIONS ON A TRIGONAL CURVE

Similar to the hyperelliptic case, the Abel image $\mathcal{A}(D)$ of a given divisor D is computed directly by the formula (36), where the Abel image $\mathcal{A}(P)$ of a point P is computed by (3) with the standard not normalized holomorphic differentials (48).

\wp -Functions are calculated on non-special divisors by means of (12). Non-special divisors D are composed as positive divisors of degree $n \geq g$ with no three points in involution on a trigonal curve of genus g .

6.1. Vector of Riemann constants. The characteristic $[K]$ of the vector of Riemann constants K is required for computation of \wp -functions by means of (12). This characteristic is half-integer, due to the relation $2K \sim \bar{\mathcal{A}}(C)$, see [14, Eq. (2.4.20)], which means that $2K$ is congruent to the Abel image of the canonical divisor C on \mathcal{C} , and the latter is congruent to zero. Recall, that $\bar{\mathcal{A}}$ denotes the Abel map with respect to normalized differentials. Moreover,

Theorem 4. *The theta function with characteristic $[K]$, as a function of not normalized coordinates u , is characterized by the maximal order \mathfrak{d} of vanishing at $u = 0$, that is*

$$\forall i < \mathfrak{d} \quad \left. \frac{\partial^i \theta[K](\omega^{-1}u)}{\partial u_1^i} \right|_{u=0} = 0, \quad \left. \frac{\partial^{\mathfrak{d}} \theta[K](\omega^{-1}u)}{\partial u_1^{\mathfrak{d}}} \right|_{u=0} \neq 0,$$

where $\mathfrak{d} = (3\mathfrak{m} + 2)\mathfrak{m}$ on a $(3, 3\mathfrak{m} + 1)$ -curve, and $\mathfrak{d} = (3\mathfrak{m} + 1)(\mathfrak{m} + 1)$ on a $(3, 3\mathfrak{m} + 2)$ -curve; the order \mathfrak{d} is computed with respect to the Sato weight.

Proof. By (8) $\theta[K]$ is connected to σ -function, which means that the both functions behave similarly at the origin $u = 0$ of $\text{Jac}(\mathcal{C})$. From [9] we know the Sato weight of σ -function:

$$\text{wgt } \sigma = -\frac{1}{24}(n^2 - 1)(s^2 - 1).$$

The negative Sato weight shows the order of vanishing at $u = 0$, that is $\mathfrak{d} = -\text{wgt } \sigma$. By direct computations, one can find, that $\text{wgt } \sigma = (3\mathfrak{m} + 2)\mathfrak{m}$ on a $(3, 3\mathfrak{m} + 1)$ -curve, and $\text{wgt } \sigma = (3\mathfrak{m} + 1)(\mathfrak{m} + 1)$ on a $(3, 3\mathfrak{m} + 2)$ -curve. \square

Corollary 1. *If the weighted order \mathfrak{p} of a derivative of $\theta[K](\omega^{-1}u)$ with respect to u is less than \mathfrak{d} , then the derivative vanishes.*

Proof. The weighted order of a derivative with respect to $u = (u_{\mathfrak{w}_1}, \dots, u_{\mathfrak{w}_g})^t$ is defined as follows

$$\mathfrak{p} = \text{ord} \frac{\partial^{p_{\mathfrak{w}_1} + \dots + p_{\mathfrak{w}_g}}}{\partial u_{\mathfrak{w}_1}^{p_{\mathfrak{w}_1}} \dots \partial u_{\mathfrak{w}_g}^{p_{\mathfrak{w}_g}}} = \sum_{i=1}^g \mathfrak{w}_i p_{\mathfrak{w}_i}.$$

All derivatives of σ -function such that $\mathfrak{p} < \mathfrak{d}$ vanish at $u = 0$, due to the Riemann vanishing theorem. \square

From the relation $[K] = [\frac{1}{2}\bar{\mathcal{A}}(C)]$ the exact location of the base-point for computation can be found. Though it is known that the base-point is located at infinity, the computational base-point is a matter of investigation. Unlike the hyperelliptic case, all paths to points in calculating Abel images are required to start at the same computational base-point on a fixed sheet.

6.2. Paths to points. Let $P_i = (x_i, y_i)$, $y_i = y_a(x_i)$. From a the Sheet n where P_i is located is identified. Let $Q_i = (e_i, y_a(e_i))$, where e_i is the x -coordinate of a branch point B_i , be in the vicinity to P_i on Sheet n . A path to P_i starts at $-\infty - i\epsilon$ on the fixed sheet, and goes to Q_i on Sheet n . Then the segment $[Q_i, P_i]$ on Sheet n is added to this path. Along the path to P_i the Abel image $\mathcal{A}(P_i)$ is computed.

Below, computation of \wp -functions is illustrated by examples.

6.3. Example 3a. On the curve (52), with the homology basis chosen as shown on fig. 10, the vector of Riemann constants has the characteristic

$$(59) \quad [K] = \begin{pmatrix} 1 & 0 & 1 \\ 0 & 1 & 1 \end{pmatrix},$$

and $\theta[K]$ vanishes to the order 5 at $u = 0$.

Recall that all branch points are located on Sheet c . Let paths to all these points start at $-\infty - i\epsilon$ on Sheet c , and reach branch points in the shortest way. Then

$$(60) \quad \begin{aligned} \omega \bar{\mathcal{A}}(C) = & \mathcal{A}_{0-,1}^{[3]} + (\mathcal{A}_{0-,1}^{[3]} + \mathcal{A}_{1,2}^{[3]}) + (\mathcal{A}_{0-,1}^{[3]} + \mathcal{A}_{1,2}^{[3]} + \mathcal{A}_{2,3}^{[1]}) \\ & + (\mathcal{A}_{0-,1}^{[3]} + \mathcal{A}_{1,2}^{[3]} + \mathcal{A}_{2,4}^{[1-2]}) + (\mathcal{A}_{0-,1}^{[3]} + \mathcal{A}_{1,2}^{[3]} + \mathcal{A}_{2,4}^{[1-2]} + \mathcal{A}_{4,6}^{[3-1]} + \mathcal{A}_{6,5}^{[1-2]}) \\ & + (\mathcal{A}_{0-,1}^{[3]} + \mathcal{A}_{1,2}^{[3]} + \mathcal{A}_{2,4}^{[1-2]} + \mathcal{A}_{4,6}^{[3-1]}) \\ & + (\mathcal{A}_{0-,1}^{[3]} + \mathcal{A}_{1,2}^{[3]} + \mathcal{A}_{2,4}^{[1-2]} + \mathcal{A}_{4,6}^{[3-1]} + \mathcal{A}_{6,7}^{[2-3]}) \\ & + (\mathcal{A}_{0-,1}^{[3]} + \mathcal{A}_{1,2}^{[3]} + \mathcal{A}_{2,4}^{[1-2]} + \mathcal{A}_{4,6}^{[3-1]} + \mathcal{A}_{6,8}^{[2-3]}) \approx \begin{pmatrix} 3.5 + 1.976806i \\ -1.5 + 2.115880i \\ 1.5 + 1.338712i \end{pmatrix}, \end{aligned}$$

and in terms of columns of the normalized periods $(1_3, \tau)$:

$$(\bar{\mathcal{A}}(C))_j = \tau_{j,1} + 2\tau_{j,2} + \tau_{j,3} + 2\delta_{j,1} - 3\delta_{j,2} + \delta_{j,3},$$

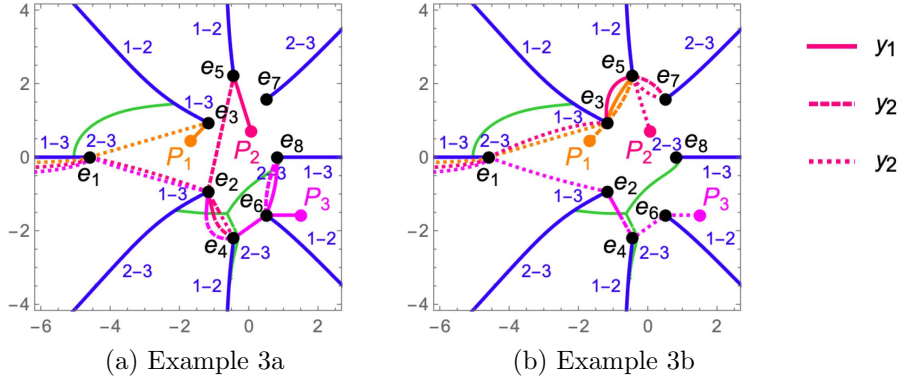
where $\delta_{i,j}$ denotes the Kronecker delta. Evidently, $\frac{1}{2}\bar{\mathcal{A}}(C)$ obtained from (60) gives the correct value of the vector of Riemann constants, since its characteristic coincides with (59). Therefore, we fix the computational base-point at $-\infty - i\epsilon$ on Sheet c .

Let a given divisor be $D = \sum_{i=1}^3 P_i$,

$$(61) \quad \begin{aligned} P_1 &= (e_3 - 0.5 - 0.5i, y_1(e_3 - 0.5 - 0.5i)) \\ &\approx (-1.679223 + 0.434455i, 3.431176 - 0.582699i), \\ P_2 &= (e_5 + 0.5 - 1.5i, y_1(e_5 + 0.5 - 1.5i)) \\ &\approx (0.068268 + 0.702564i, 3.555003 + 0.889027i), \\ P_3 &= (e_6 + 1, y_1(e_6 + 1)) \\ &\approx (1.499118 - 1.575269i, -4.191263 + 1.058317i). \end{aligned}$$

The points P_1 and P_3 are located on Sheet a , and P_2 on Sheet b . A path to each point starts at $-\infty - i\epsilon$ on Sheet c . Let P_1 on Sheet a be reached through the cut (B_2, B_3) , then P_2 on Sheet b through the cut (B_4, B_5) , and P_3 on Sheet a through the cut $(B_8, \infty) \cup (\infty, B_1)$, see fig. 11(a). Actually,

$$\mathcal{A}(P_1) = \mathcal{A}_{0-,1}^{[3]} + \mathcal{A}_{1,3}^{[3]} + \int_{e_3}^{P_1} du^{[1]},$$

FIGURE 11. Paths to points of divisor D .

$$\mathcal{A}(P_2) = \mathcal{A}_{0,-,1}^{[3]} + \mathcal{A}_{1,2}^{[3]} + \mathcal{A}_{2,4}^{[1-2]} + \mathcal{A}_{4,2}^{[3-2]} + \mathcal{A}_{2,5}^{[2]} + \int_{e_5}^{P_2} du^{[1]},$$

$$\mathcal{A}(P_3) = \mathcal{A}_{0,-,1}^{[3]} + \mathcal{A}_{1,2}^{[3]} + \mathcal{A}_{2,4}^{[1-2]} + \mathcal{A}_{4,6}^{[3-1]} + \int_{e_6}^{P_3} du^{[1]},$$

where $du^{[a]}$ means that $y = y_a(x)$. The Abel image of D is

$$(62) \quad u(D) = \sum_{i=1}^3 \mathcal{A}(P_i) \approx \begin{pmatrix} -0.270333 - 1.612257i \\ -1.116879 + 0.562199i \\ 0.258194 + 0.268653i \end{pmatrix}.$$

By means of (12), with θ -function approximated by a partial sum of (6), $n_i \leq 5$, we obtain

$$(63) \quad \begin{aligned} \wp_{1,1}(u(D)) &\approx 0.059654 + 1.020925i, \\ \wp_{1,2}(u(D)) &\approx -0.793416 + 0.889005i, \\ \wp_{1,5}(u(D)) &\approx 0.885372 - 3.089764i, \\ \wp_{2,2}(u(D)) &\approx -0.269700 + 1.472739i, \\ \wp_{2,5}(u(D)) &\approx -3.501466 + 10.538856i, \\ \wp_{1,1,1}(u(D)) &\approx -2.156576 + 3.543516i, \\ \wp_{1,1,2}(u(D)) &\approx -3.595029 + 2.840859i, \\ \wp_{1,1,5}(u(D)) &\approx 5.656516 - 0.559812i. \end{aligned}$$

Alternatively, a part of the path $\bar{\gamma}_{3\infty}$ around infinity can be used to reach each point on its sheet avoiding cuts. Denote

$$\begin{aligned} \mathcal{A}(\tilde{\gamma}_L^c) &= \mathcal{A}_{1,2}^{[3]} + \mathcal{A}_{2,4}^{[1-2]} + \mathcal{A}_{4,6}^{[3-1]} + \mathcal{A}_{6,8}^{[2-3]}, \\ \mathcal{A}(\tilde{\gamma}_L^a) &= \mathcal{A}_{1,2}^{[1]} + \mathcal{A}_{2,4}^{[3-1]} + \mathcal{A}_{4,6}^{[1-2]} + \mathcal{A}_{6,8}^{[1-2]}, \\ \mathcal{A}(\tilde{\gamma}_L^b) &= \mathcal{A}_{1,2}^{[2]} + \mathcal{A}_{2,4}^{[2-3]} + \mathcal{A}_{4,6}^{[2-3]} + \mathcal{A}_{6,8}^{[3-1]}, \\ \mathcal{A}(\tilde{\gamma}_U^a) &= \mathcal{A}_{8,7}^{[2]} + \mathcal{A}_{7,5}^{[3]} + \mathcal{A}_{5,3}^{[3]} + \mathcal{A}_{3,1}^{[1]}, \\ \mathcal{A}(\tilde{\gamma}_U^c) &= \mathcal{A}_{8,7}^{[1]} + \mathcal{A}_{7,5}^{[1]} + \mathcal{A}_{5,3}^{[2]} + \mathcal{A}_{3,1}^{[2]}, \end{aligned}$$

$$\mathcal{A}(\tilde{\gamma}_U^b) = \mathcal{A}_{8,7}^{[3]} + \mathcal{A}_{7,5}^{[2]} + \mathcal{A}_{5,3}^{[1]} + \mathcal{A}_{1,3}^{[3]},$$

cf. (57) and (58), then

$$\begin{aligned}\mathcal{A}(\tilde{\gamma}_\infty^{c-a}) &= \mathcal{A}(\tilde{\gamma}_L^c) + \mathcal{A}(\tilde{\gamma}_U^a), \\ \mathcal{A}(\tilde{\gamma}_\infty^{a-c}) &= \mathcal{A}(\tilde{\gamma}_L^a) + \mathcal{A}(\tilde{\gamma}_U^c), \\ \mathcal{A}(\tilde{\gamma}_\infty^{b-b}) &= \mathcal{A}(\tilde{\gamma}_L^b) + \mathcal{A}(\tilde{\gamma}_U^b).\end{aligned}$$

$\mathcal{A}(\tilde{\gamma}_L^c)$ can be used to reach the vicinity of B_8 on Sheet a, and $\mathcal{A}(\tilde{\gamma}_\infty^{c-a})$ to reach the vicinity of B_1 on Sheet a. By $\mathcal{A}(\tilde{\gamma}_\infty^{c-a}) + \mathcal{A}(\tilde{\gamma}_\infty^{a-c})$ the vicinity of B_1 on Sheet b can be reached, and by $\mathcal{A}(\tilde{\gamma}_\infty^{c-a}) + \mathcal{A}(\tilde{\gamma}_\infty^{a-c}) + \mathcal{A}(\tilde{\gamma}_L^b)$ the vicinity of B_8 on Sheet b. Then

$$\begin{aligned}\mathcal{A}(P_1) &= \mathcal{A}_{0-,1}^{[3]} + \mathcal{A}(\tilde{\gamma}_\infty^{c-a}) + \mathcal{A}_{1,3}^{[1]} + \int_{e_3}^{P_1} du^{[1]}, \\ \mathcal{A}(P_2) &= \mathcal{A}_{0-,1}^{[3]} + \mathcal{A}(\tilde{\gamma}_\infty^{c-a}) + \mathcal{A}(\tilde{\gamma}_\infty^{a-c}) + \mathcal{A}_{1,2}^{[2]} + \mathcal{A}_{2,4}^{[2-3]} + \mathcal{A}_{4,6}^{[2-3]} + \mathcal{A}_{6,5}^{[3-1]} + \int_{e_5}^{P_2} du^{[1]}, \\ \mathcal{A}(P_3) &= \mathcal{A}_{0-,1}^{[3]} + \mathcal{A}(\tilde{\gamma}_\infty^{c-a}) + \mathcal{A}_{1,2}^{[1]} + \mathcal{A}_{2,4}^{[3-1]} + \mathcal{A}_{4,6}^{[1-2]} + \int_{e_6}^{P_3} du^{[1]},\end{aligned}$$

which produce an Abel image congruent to (62), namely

$$(64) \quad u(D) = \sum_{i=1}^3 \mathcal{A}(P_i) \approx \begin{pmatrix} -0.546310 + 0.440673i \\ 0.496998 - 0.233192i \\ 0.028495 - 0.067950i \end{pmatrix}.$$

Values of \wp -functions on (64) and (62) coincide with an accuracy of 10^{-13} .

A solution of the Jacobi inversion problem on a (3, 4)-curve (52) is given by the system

$$(65a) \quad \mathcal{R}_6(x, y; u) \equiv x^2 - y\wp_{1,1}(u) - x\wp_{1,2}(u) - \wp_{1,5}(u) = 0,$$

$$(65b) \quad \mathcal{R}_7(x, y; u) \equiv 2xy + y(\wp_{1,1,1}(u) - \wp_{1,2}(u)) \\ + x(\wp_{1,1,2}(u) - \wp_{2,2}(u)) + (\wp_{1,1,5}(u) - \wp_{2,5}(u)) = 0,$$

whose divisor of zeros is a degree 3 positive divisor D_3 such that $u = \mathcal{A}(D_3)$.

On the other hand, the two polynomial functions \mathcal{R}_6 and \mathcal{R}_7 on a (3, 4)-curve (52) can be constructed directly from coordinates of points of a degree 3 divisor $D_3 = \sum_{i=1}^3 (x_i, y_i)$. Namely,

$$(66) \quad \mathcal{R}_6(x, y; D_3) = \frac{\begin{vmatrix} x^2 & y & x & 1 \\ x_1^2 & y_1 & x_1 & 1 \\ x_2^2 & y_2 & x_2 & 1 \\ x_3^2 & y_3 & x_3 & 1 \end{vmatrix}}{\begin{vmatrix} y_1 & x_1 & 1 \\ y_2 & x_2 & 1 \\ y_3 & x_3 & 1 \end{vmatrix}}, \quad \mathcal{R}_7(x, y; D_3) = 2 \frac{\begin{vmatrix} xy & y & x & 1 \\ x_1y_1 & y_1 & x_1 & 1 \\ x_2y_2 & y_2 & x_2 & 1 \\ x_3y_3 & y_3 & x_3 & 1 \end{vmatrix}}{\begin{vmatrix} y_1 & x_1 & 1 \\ y_2 & x_2 & 1 \\ y_3 & x_3 & 1 \end{vmatrix}}.$$

On the given divisor D defined by (61) we obtain

$$\begin{aligned}\mathcal{R}_6(x, y; D) &= x^2 - (0.059654 + 1.020925i)y \\ &\quad + (0.793416 - 0.889005i)x - 0.885372 + 3.089764i, \\ \mathcal{R}_7(x, y; D) &= 2xy - (1.363160 - 2.654511i)y \\ &\quad - (3.325329 - 1.368120i)x + 9.157983 - 11.098669i.\end{aligned}$$

Coefficients of these two functions coincide with those expressed in terms of \wp -functions (63) within an accuracy of 10^{-13} .

6.4. Example 3b. Let D be slightly modified by choosing points with the same x -coordinates, but located on other sheets, namely

$$\begin{aligned}
P_1 &= (e_3 - 0.5 - 0.5\iota, y_2(e_3 - 0.5 - 0.5\iota)) \\
&\approx (-1.679223 + 0.434455\iota, -3.855009 + 0.446784\iota), \\
P_2 &= (e_5 + 0.5 - 1.5\iota, y_3(e_5 + 0.5 - 1.5\iota)) \\
&\approx (0.068268 + 0.702564\iota, -0.916997 - 0.935049\iota), \\
P_3 &= (e_6 + 1, y_3(e_6 + 1)) \\
&\approx (1.499118 - 1.575269\iota, 5.701625 - 3.318255\iota).
\end{aligned}
\tag{68}$$

The points P_1 and P_3 are located on Sheet **b**, and P_2 on Sheet **a**. Let P_1 and P_3 on Sheet **b** be reached through the cut (B_4, B_5) , and P_2 on Sheet **a** through the cut (B_6, B_7) , see fig. 11(b). Actually,

$$\begin{aligned}
\mathcal{A}(P_1) &= \mathcal{A}_{0-,1}^{[3]} + \mathcal{A}_{1,3}^{[3]} + \mathcal{A}_{3,5}^{[1]} + \mathcal{A}_{5,3}^{[2]} + \int_{e_3}^{P_1} du^{[2]}, \\
\mathcal{A}(P_2) &= \mathcal{A}_{0-,1}^{[3]} + \mathcal{A}_{1,3}^{[3]} + \mathcal{A}_{3,5}^{[1]} + \mathcal{A}_{5,7}^{[2]} + \mathcal{A}_{7,5}^{[3]} + \int_{e_5}^{P_2} du^{[3]}, \\
\mathcal{A}(P_3) &= \mathcal{A}_{0-,1}^{[3]} + \mathcal{A}_{1,2}^{[3]} + \mathcal{A}_{2,4}^{[1-2]} + \mathcal{A}_{4,6}^{[2-3]} + \int_{e_6}^{P_3} du^{[3]}.
\end{aligned}$$

The Abel image of D is

$$\mathcal{A}(D) = \sum_{i=1}^3 \mathcal{A}(P_i) \approx \begin{pmatrix} -0.421105 - 2.303962\iota \\ -1.319230 - 1.997581\iota \\ -0.176345 + 0.125109\iota \end{pmatrix},
\tag{69}$$

and \wp -functions acquire the following values

$$\begin{aligned}
\wp_{1,1}(u(D)) &\approx -0.497171 - 1.306218\iota, \\
\wp_{1,2}(u(D)) &\approx 0.485105 + 2.618402\iota, \\
\wp_{1,5}(u(D)) &\approx 2.083016 - 2.086324\iota, \\
\wp_{2,2}(u(D)) &\approx -2.356414 + 10.869587\iota, \\
\wp_{2,5}(u(D)) &\approx 15.590831 + 2.902800\iota, \\
\wp_{1,1,1}(u(D)) &\approx 1.678988 + 8.731706\iota, \\
\wp_{1,1,2}(u(D)) &\approx -4.377331 - 0.119524\iota, \\
\wp_{1,1,5}(u(D)) &\approx 2.198126 + 13.211222\iota.
\end{aligned}
\tag{70}$$

With these values the two functions $\mathcal{R}_6, \mathcal{R}_7$ in (65) are constructed.

On the other hand, the two polynomial functions $\mathcal{R}_6, \mathcal{R}_7$ are obtained by (66) from coordinates of the given divisor D defined by (68), namely

$$\begin{aligned}
\mathcal{R}_6(x, y; D) &= x^2 + (0.497171 + 1.306218\iota)y \\
&\quad - (0.485105 + 2.618402\iota)x - 2.083016 + 2.086324\iota, \\
\mathcal{R}_7(x, y; D) &= 2xy + (1.193883 + 6.113304\iota)y
\end{aligned}$$

$$- (2.020917 + 10.989112i)x - 13.392705 + 10.308422i.$$

Coefficients of these two functions coincide with those computed from \wp -functions (70) within an accuracy of 10^{-9} .

7. ACKNOWLEDGMENTS

The present paper was inspired by S. Matsutani, who expressed an active interest into analytical computation of \wp -functions in Mathematica.

REFERENCES

- [1] Agostini D., Chua L., Computing theta functions with Julia, *Journal of Software for Algebra and Geometry* **11** (2021) pp. 41–51.
- [2] Baker H.F., *Abelian functions: Abel’s theorem and the allied theory of theta functions*, Cambridge Univ. Press, Cambridge, 1897.
- [3] Baker H.F., *Multiply periodic functions*, Cambridge Univ. Press, Cambridge, 1907.
- [4] Belokolos E. D., Bobenko A. I., Enolski V. Z., Its A. R., Matveev. V.B., *Algebro-geometric approach to nonlinear integrable equations*, Springer Series in Nonlinear Dynamics, Springer, Berlin, 1994.
- [5] Bernatska J., General derivative Thomae formula for singular half-periods, *Lett. Math. Phys.* **110** (2020) pp. 2983–3014; arXiv:1904.09333 [math.AG]
- [6] Bernatska J., Reality conditions for the KdV equation and exact quasi-periodic solutions in finite phase spaces, *J. Geom. Phys.* **206** (2024) 105322; arXiv:2312.10859.
- [7] Bernatska J., Leykin D., Solution of the Jacobi inversion problem on non-hyperelliptic curves, *Lett. Math. Phys.* **113** (2023) 110; arXiv:2212.14492
- [8] Bolza O., Ueber die Reduction hyperelliptischer Integrale erster Ordnung und erster Gattung auf elliptische durch eine Transformation vierten Grades, *Math. Ann.* **28**:3 (1887) pp. 447–456.
- [9] Buchstaber V. M., Enolskii V. Z., Leykin D. V., *Rational analogs of abelian functions*, *Functional Analysis and Its Applications*, **33**:2 (1999) pp. 83–94.
- [10] Buchstaber V. M., Enolskii V. Z., and Leykin D. V., *Hyperelliptic Kleinian Functions and Applications*, preprint ESI 380, Vienna, 1996.
- [11] Buchstaber V. M., Enolskii V. Z., Leykin D. V., Uniformization of Jacobi varieties of trigonal curves and nonlinear differential equations, *Functional Analysis and Its Applications* **34** (2000) pp. 159–171.
- [12] Deconinck B., van Hoeij M., Computing Riemann matrices of algebraic curves, *Physica D* **152–153** (2001) pp. 28–46.
- [13] Deconinck B., Patterson M. S., Computing with plane algebraic curves and Riemann surfaces: The algorithms of the Maple package “Algcurves” in *Computational approach to Riemann surfaces* (Lect. Notes Math. Vol. 2013), eds. Bobenko A. I., Klein C., Springer, Berlin, 2011.
- [14] Dubrovin B. A., Theta functions and non-linear equations, *Russ. Math. Surv.* **36**:2 (1981) pp. 11–80.
- [15] Enolski V.Z., Richter P.H., Periods of hyperelliptic integrals expressed in terms of θ -constants by means of Thomae formulae. *Phil. Trans. London Math. Soc. A* **366** (2008) pp. 1005–1024.
- [16] Fay J. D., *Theta functions on Riemann surfaces*, *Lectures Notes in Mathematics*, Vol. 352, Springer, Berlin, 1973.
- [17] Frauendiener J., Klein C., Hyperelliptic theta-functions and spectral methods, *Journal of Computational and Applied Mathematics* **167** (2004) pp. 193–218.
- [18] Frauendiener J., Klein C., Hyperelliptic theta-functions and spectral methods: KdV and KP solutions, *Lett. Math. Phys.* **76** (2006) pp. 249–267.
- [19] Kalla C., Klein C., On the numerical evaluation of algebro-geometric solutions to integrable equations, *Nonlinearity* **25** (2012) pp. 569–596.
- [20] Matsutani S., Previato E., An algebro-geometric model for the shape of supercoiled DNA, *Physica D* **430** (2022) 133073.
- [21] Matsutani S., A graphical representation of hyperelliptic KdV solutions, *Communications in Nonlinear Science and Numerical Simulation* **138** (2024) 108259; arXiv:2310.14656